Volume 48, Number 1, 2022.

Mobility & Vehicle Mechanics

International Journal for Vehicle Mechanics, Engines and Transportation Systems

ISSN 1450 - 5304

UDC 621 + 629(05)=802.0

UNIVERSITY OF KRAGUJEVAC, FACULTY OF ENGINEERING

SERBIAN SOCIETY OF AUTOMOTIVE ENGINEERS

M V M **M**obility **V**ehicle **M**echanics

Editors: Prof. dr ***Jovanka Lukić****; Prof. dr* ***Čedomir Duboka***

For Publisher: Prof. dr Dobrica Milovanović, dean, University of Kragujevac, Faculty of Engineering

Publishing of this Journal is financially supported from:
Ministry of Education, Science and Technological Development, Republic Serbia

Mobility &		**M**otorna
Vehicle	**Volume 48** **Number 1** **2022.**	**V**ozila i
Mechanics		**M**otori

Mobility & **V**ehicle **M**echanics

Motorna **V**ozila i **M**otori

Volume 48
Number 1
2022.

MOBILITY & VEHICLE MECHANICS

DOI: 10.24874/mvm.2022.48.01.01
UDC: 629.3.077

CONTRIBUTION TO THE RESEARCH OF AN ACCEPTABLE TEST FOR THE IDENTIFICATION OF THE BEHAVIOR PARAMETERS OF TRUCK VEHICLE

Miroslav Demić [1]*, *Aleksandar Đurić* [2], *Aleksandar Grkić* [3], *Momir Drakulić* [4], *†Slavko Muždeka* [5]

Received in March 2022 *Accepted in April 2022*

RESEARCH ARTICLE

ABSTRACT: The design of engine vehicles cannot be imagined without considering the mutual relations in the complex dynamic system Driver - Vehicle - Environment. Inconsistency between any of the connections in the mentioned system leads to disruption in the functioning of the system as a whole, which in some cases can lead to catastrophic consequences. The necessity of knowing the parameters of behavior on the road for traffic safety is especially emphasized. Therefore, in practice, it is researched in different conditions. It was considered expedient to establish the reliability of some tests used during the research of truck behavior on the road. A detailed analysis, based on the study of the interdependencies of the controlled (steering wheel angle and torque at the steering wheel) and partially controlled excitation (vehicle velocity) concluded that the overtaking test is the most acceptable for these researces.

KEY WORDS: *truck vehicle, road behaviour, tests*

[1]*Miroslav Demić, PhD, Engineering science academy of Serbia, Belgrade, Serbia, Kraljice Marije 16, soba 218a, Belgrade, Serbia (*Corresponding author), demic@kg.ac.rs, https://orcid.org/0000-0003-2168-1370*

[2]*Aleksandar Đurić, MSc, University of defense, Military academy, Department of military mechanical engineering, Veljka Lukica Kurjaka 33, Belgrade, Serbia, aleksandar_djrc@yahoo.com, https://orcid.org/0000-0002-2165-528X*

[3]*Aleksandar Grkić, AMSS, Center for motor vehicles, Kneginje Zorke 58, Belgrade, Serbia, aleksandargrkic@gmail.com, https://orcid.org/0000-0002-7890-1787*

[4]*Momir Drakulić,* University of defense, *Military academy, Department of military mechanical engineering, Veljka Lukica Kurjaka 33, Belgrade, Serbia, drakulic.momir@gmail.com, https://orcid.org/0000-0002-8367-7281*

[5]*Slavko Muždeka, PhD, University of defense, Military academy, Department of military mechanical engineering, Veljka Lukica Kurjaka 33, Belgrade, Serbia, https://orcid.org/0000-0002-6189-9473*

PRILOG ISTRAŽIVANJU PRIHVATLJIVOG TESTA ZA IDENTIFIKACIJU PARAMETARA PONAŠANJA TERETNOG MOTORNOG VOZILA NA PUTU

REZIME: Projektovanje motornih vozila se ne može zamisliti bez sagledavanja međusobnih relacija u složenom dinamičkom sistemu Vozač – Vozilo – Okruženje. Neusaglašenost između bilo koje od veza u pomenutom sistemu, dovodi do poremećaja u funkcionisanju sistema kao celine, a što u nekim slučajevima može dovesti i do katastrofalnih posledica. Ovde se posebno ističe neophodnost poznavanja parametara ponašanjana na putu za bezbednost saobraćaja. Zbog toga se u praksi vrši istraživanje istog u različitim uslovima. Ocenjeno je celishodnim da se ustanovi pouzdanost nekih testova koji se koriste tokom istraživanja ponašanja kamiona na putu. Detaljnom analizom, zasnovanom na istraživanju međusobnih zavisnosti kontrolisanih (ugao i moment na točku upravljača) i delimično kontrolisane pobude (brzina) zaključeno da je test preticanja najprihvatljiviji za ta ispitivanja.

KLJUČNE REČI: *teretno motorno vozilo, ponašanje na putu, testovi*

CONTRIBUTION TO THE RESEARCH OF AN ACCEPTABLE TEST FOR THE IDENTIFICATION OF THE BEHAVIOR PARAMETERS OF TRUCK VEHICLE

Miroslav Demić, Aleksandar Đurić, Aleksandar Grkić, Momir Drakulić, Slavko Muždeka

INTRODUCTION

In order to systematically study the relationship in the Driver-Vehicle-Environment system (DVE), it is necessary to adopt a methodology. The most acceptable methodology is based on automatic control, in which the vehicle is presented as a system composed of different subsystems. These subsystems may or may not be isolated from each other [1-3]. In the abundance of literature data on possible DVE connections [1-8], it was considered expedient to present a simple scheme [4], Figure 1.

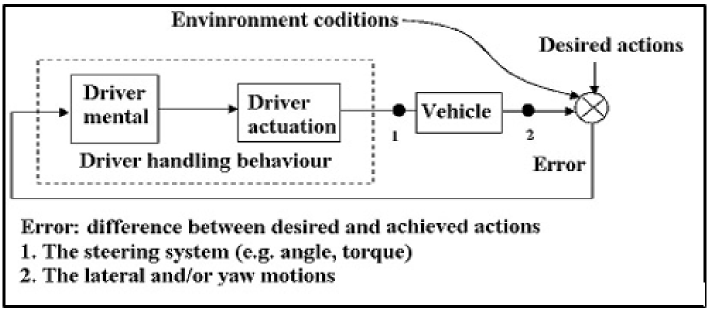

Figure 1 Control system: Driver-Vehicle-Environment

The driver follows the desired trajectory and compares it with the wanted one. He also has in mind the conditions imposed by the environment (width of the road, curvature, obstacle on the road, or the existence of crosswinds). Regardless of this information, the driver continuously receives information about the vehicle, such as velocity, rpm and engine temperature, steering wheel rotation angle, etc.

The driver's main goal is to keep the vehicle on the road and on a precisely defined path. To succeed in this, he must adjust the vehicle velocity to the condition of the road and drive the vehicle according to his driving skills. Adequate driving speed depends on the road conditions in which the vehicle is moving.

Having in mind the road conditions, the driver acts on the vehicle controls in accordance with the information he has, and in [3], they are categorized as controlled (steering wheel angle and torque on it), partially controlled (vehicle velocity), or insufficiently / not controlled influences (micro and macro road relief, wind, etc.). There are several papers in the contemporary literature that consider this problem [1-8].

The vehicle is a member of a cybernetic system that is regulated by the driver will [1]. Therefore, it is important to investigate its dynamic characteristics, and especially the characteristics of road behavior. In order to identify the dynamic parameters of vehicle behavior on the road in general, three approaches are used, namely [9-19]:

- Experimental;
- Dynamic simulation using vehicle models;

- Combination of the first two methods.

As is known [9-19], each of these approaches has its advantages and disadvantages. Bearing in mind that this is explained in detail in the mentioned references, there will be no more talk about it. In the general case, the movement of vehicles is done on uneven roads and curvilinear paths in the level of roads. The path can be identified on the basis of its spatial geometry (macro-relief) and micro-roughness (micro-relief) [20-24]. In order to soften the impact of road parameters on registered values, all research was conducted on the airfield runway near Belgrade, that has same characteristics of micro-roughness in width and length.

This paper will discuss the research of an acceptable test for the identification of vehicle behaviour parameters on the road. Special attention is paid on tests: rectilinear driving test, DLC test and overtaking test.

1. EXPERIMENT

As mentioned, the aim of the research was to establish acceptable tests for determine behavior parameters of the FAP 1118 truck on the road. The mentioned truck had a 4x4 drive formula and a load capacity of 4 t. The maximum weight of the test vehicle is 11000 kg, and during the test the vehicle was partially loaded (weight 7800 kg). The measuring chain for measuring the dynamic parameters of the vehicle consisted of the following elements:

- Kistler Correvit S-350 sensors for direct, slip-free measurement of longitudinal and transverse vehicle dynamic;
- HBM Quantum MX 840B universal measuring acquisition system;
- B-12 acceleration sensor, located in the center of gravity of the rear truck bridge;
- SST 810 dynamic inclinometer, placed in the center of gravity of the vehicle. With it, angle, velocity and acceleration was measured around the X, Y and Z axes of the vehicle;
- Steering wheel shaft angle and torque sensor.

The scheme of measuring points is given in Figure 2.

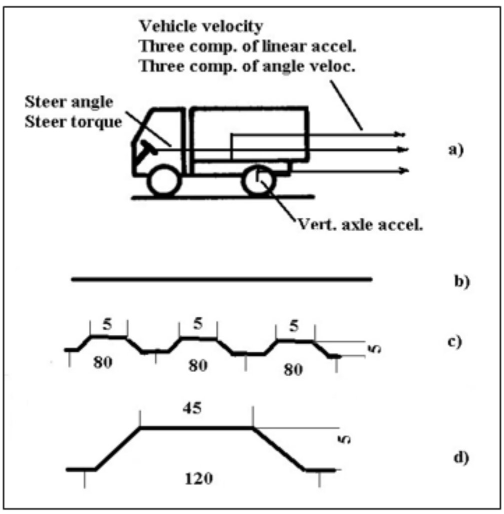

Figure 2 a)Diagram of measuring points during the FAP 1118 vehicle behavior test b)sketch of overtaking test; c), sketch of DLC test; d) rectilinear driving- dimensions, [m] It must be noted that the experiment included the registration of a number of values, but in this paper were analyzed separately: steering wheel angle and steering wheel torque, vehicle velocity and as most important, road behavior parameters [3], lateral vehicle acceleration and yaw. Based on previous experiences at the Military Academy, it was considered expedient to test the vehicle in following conditions:

- Rectilinear driving test with both hands on steering wheel (with maximum vehicle speed 30 km / h);
- DLC test (with maximum vehicle speed 45 km / h);
- overtaking test (with maximum vehicle speed 45 km / h).

The tests were performed on the base of the airport near Belgrade, and a sketch of the test route is given in Figures 2b, 2c and 2d. During the experiment, driver controlled variables (angle and torque at steering wheel), partially controlled variables (velocity) and variable close related to a micro relief of the road (acceleration of the vehicle's rear axle center) were registered [3, 25]. For the illustration, Figure 3 shows the time histories of the mentioned excitations during the overtaking test. Their change in the time domain is clearly visible.

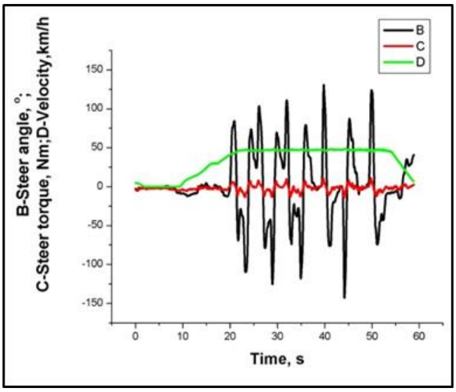

Figure 3 Time history of registered input values during the overtaking test

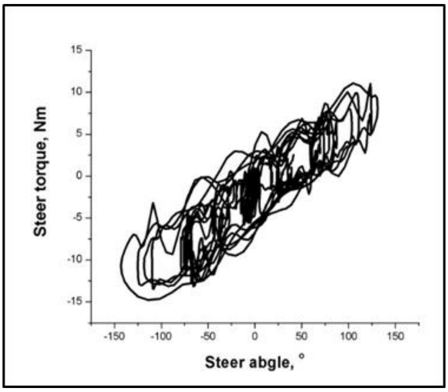

Figure 4 Couple: Steer angle – Torque at steering wheel during overtaking test

It was considered expedient to show the interdependencies of controlled and partially controlled input quantities, Figures 4, 5 and 6.

Based on Figures 4-6, it can be argued that there are links between driver motivations, which will be discussed later. For further analysis, Figure 7 shows the time changes of the lateral acceleration of the center of gravity and the angular velocity of the vehicle yaw.

From Figure 7 it can be determined that the observed parameters of the vehicle center of gravity during the overtaking test depend on time and that they belong to the group of random processes, which analysis will be performed later.

In order to determine an acceptable test to investigate the behavior of the truck on the road, accelerated tests were performed during its movement on a straight path, during the DLC test and overtaking test.

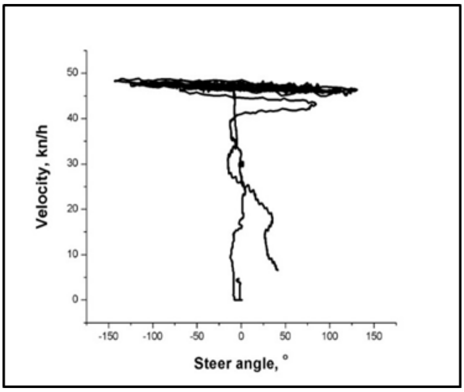

Figure 5 Couple: Angle of steering wheel – vehicle velocity during overtaking test

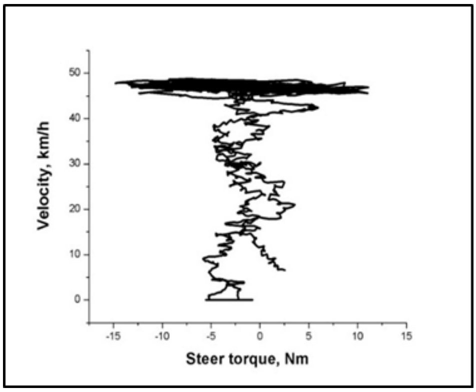

Figure 6 Couple: Torque to steering wheel – vehicle velocity during overtaking test

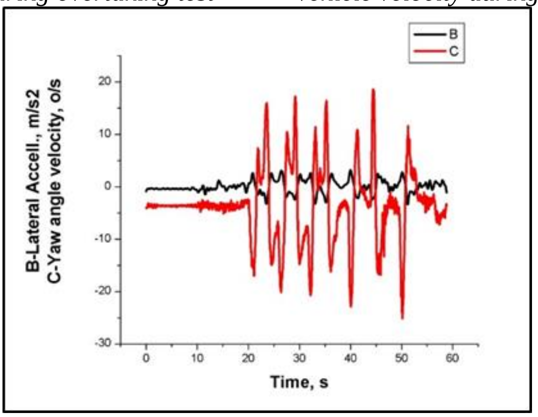

Figure 7 Lateral acceleration and angular yaw velocity of the truck during the overtaking test

2. DATA ANALYSIS

As the discretization was performed at 50 Hz and depending on the test, at at least 1024 points, the frequency range is 0.05 to 25 Hz [26-29]. The analysis of random and bias errors, for the number of data used, showed that a sufficient number of averaging of 100 (for autonomous signal) and 138 for coupled values, which achieves a minimum reliable frequency of 0.073, which is acceptable in our case [26-28]. Frequency analysis was performed for all observed excitations in the range 0.08 to 25 Hz, but it was considered expedient to graphically display spectrum modules up to about 1.1 Hz [3] in the case of controlled and partially controlled excitations, (which is illustrated in Figures 8-10 , for the overtaking test).

Analyzes of the calculated spectrum modules for all tests showed that their maximum amplitudes of angle and torque at the steering wheel and vehicle velocity were in the range up to about 0.5 Hz. This points to the need for further analyzes to be conducted for lower frequencies, e.g. up to a maximum of 1.1 Hz, which is in accordance with [3].

Having in mind Figures 4-6 which show interdependencies, it was considered expedient to determine the extent to which there is a statistical link between registered controlled and partially controlled excitations [26-28]. In this sense, the functions of ordinary coherences were calculated, using the *Demparcoh* program [29] and shown in Figures 11, 12 and 13.

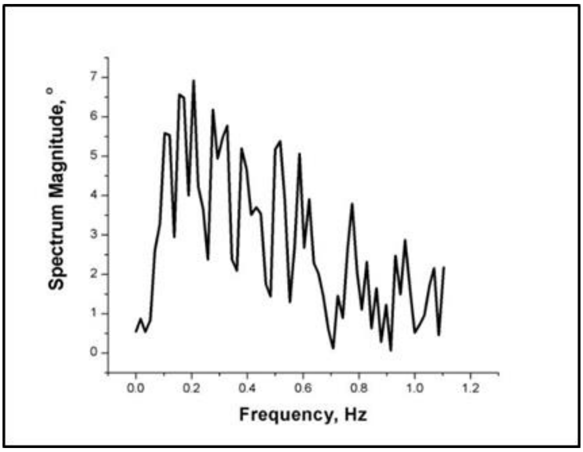

Figure 8 The magnitude of the steering angle amplitude spectrum during the overtaking test

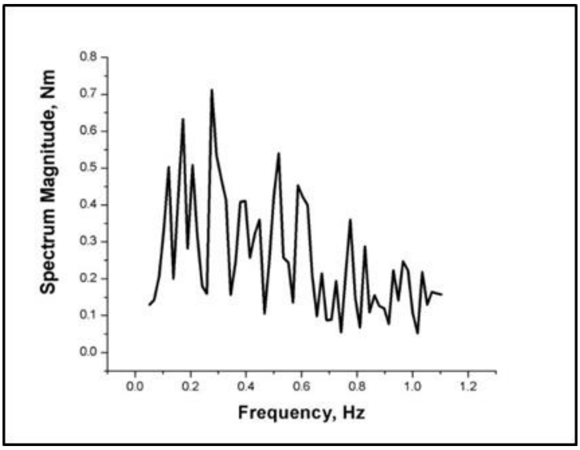

Figure 9 The magnitude of the torque amplitude spectrum at the steering wheel during the overtaking test

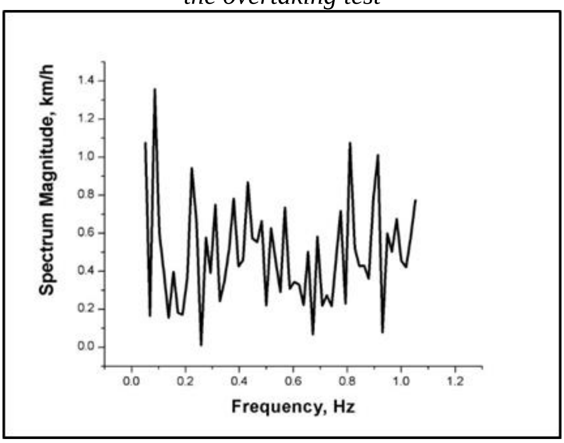

Figure 10 Velocity spectrum magnitude during overtaking test

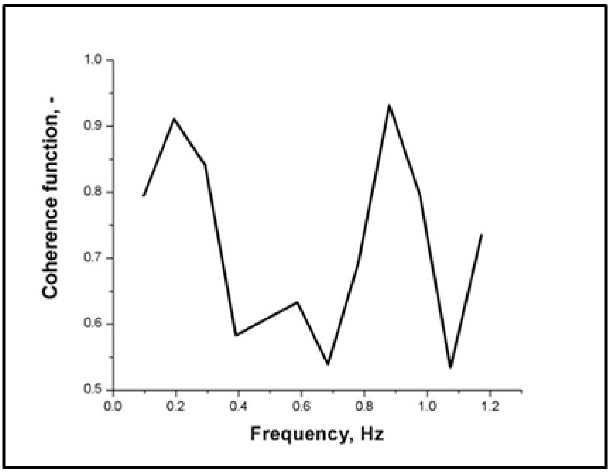

Figure 11 Coherence: Angle of steering wheel– torque at steering wheel during overtaking test

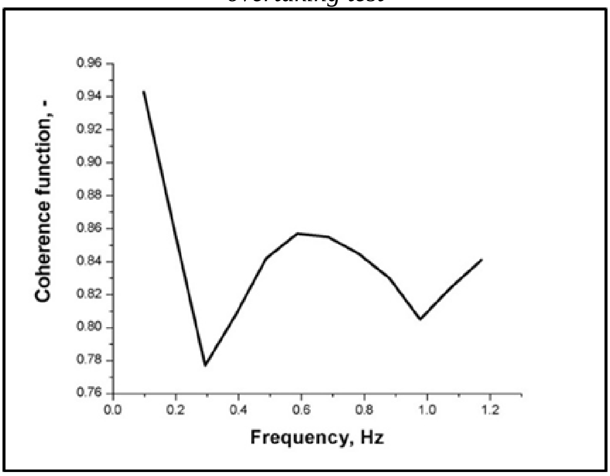

Figure 12 Coherence: Angle of steering wheel – vehicle velocity during overtaking test

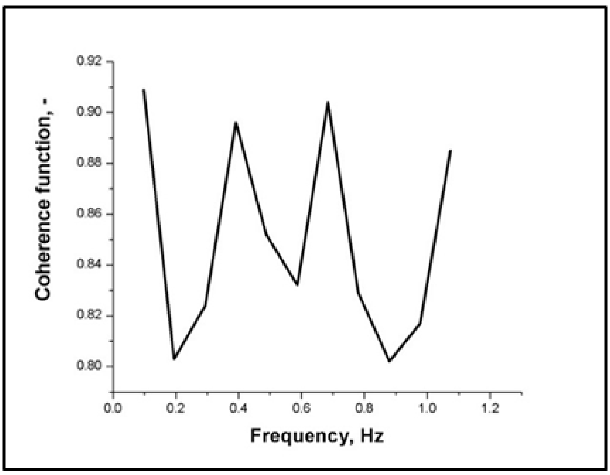

Figure 13 Coherence: Torque at steering wheel – vehicle velocity during overtaking test

The analysis of Figures 11-13 showed that the coherence in the characteristic range up to 1.1 Hz is in the range 0.55 to close to 0.94, which shows that the selected excitations are not independent [26-28], so this must be kept in mind during the analysis.

For the purpose of further analysis, it was considered expedient to calculate cross-spectra of registered values [26-28], using the software Analsigdem [29]:

- steering wheel angle – lateral acceleration and yaw;
- torque at steering wheel - lateral acceleration and yaw;
- vehicle velocity – lateral acceleration and yaw.

As is known, cross-spectra represent a quantity that indicates whether there is a relationship between the observed pairs of quantities [26-28]. For illustration, the following are the cross-spectrum modules: steering wheel angle - lateral acceleration and yaw (Figure 14), torque at steering wheel - lateral acceleration and yaw (Figure 15) and vehicle velocity - lateral acceleration and yaw (Figure 16), during the DLC test. By analyzing all the data, partially shown in Figures 14-16, it was found that there is a coupling between input (steering wheel angle, torque at steering wheel, vehicle velocity) and output values (lateral acceleration and yaw). However, it should be borne in mind that the measured lateral accelerations and yaw are functions of simultaneous driver action on the steering wheel (angle, torque) and fuel slipper, so that based on cross-spectrum can not distinguish influence of separate values to output excitations. All the more so because we have shown that the adopted inputs are not independent, but that there is a connection between them, which was discussed earlier. It was considered expedient to perform an additional analysis based on the so-called partial coherence functions [26-28]. Therefore, we will briefly present the theory of signal decoupling, on the example of three, interconnected input values [26-28].

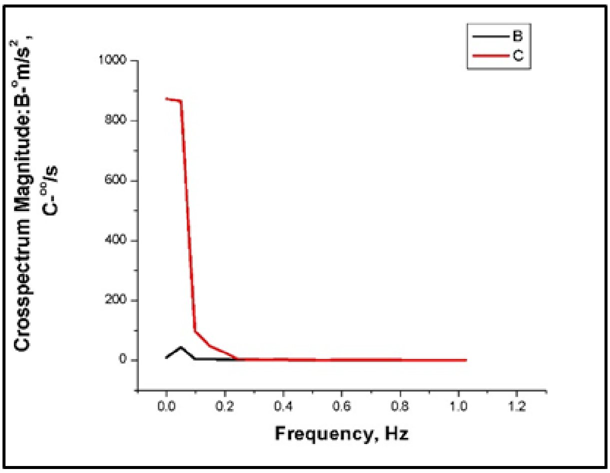

Figure 14 Cros-spectra: steering wheel angle – lateral acceleration, steering wheel angle -yaw during DLC test

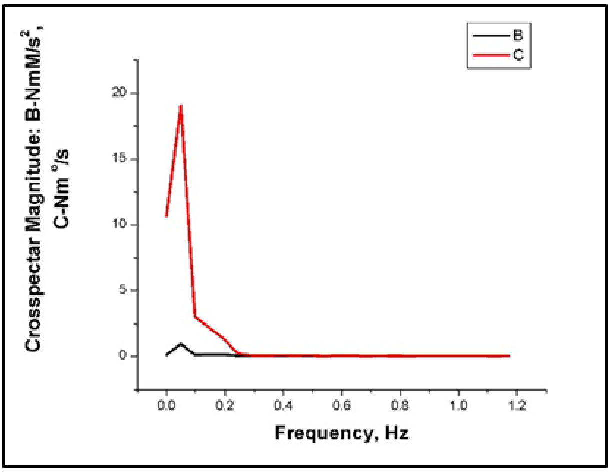

Figure 15 Cros-spectra: Torque at steering wheel – lateral acceleration, Torque at steering wheel -yaw during DLC test

8 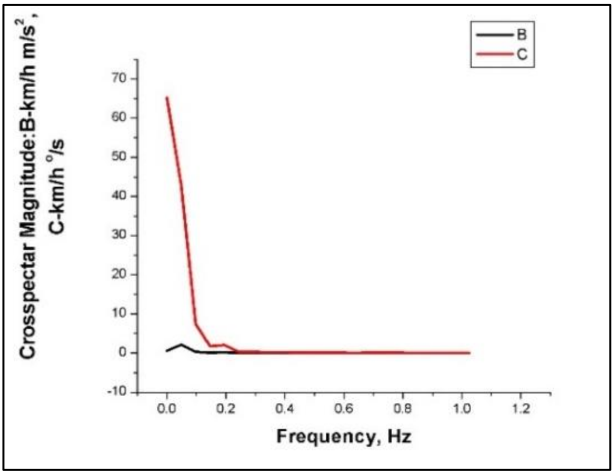

Figure 16 Cros-spectra: Velocity – lateral acceleration, Velocity -yaw during DLC test

The problem is schematically shown in Figure 17. Figure 17a shows that, in terms of regulation, the problem belongs to the group of systems with multiple inputs and outputs, which is presented to systems with multiple inputs and one output for easier solution, Figure 17b [26-28]. It is obvious from the picture that each individual output variable can be observed as a function of input variables, which are correlated.

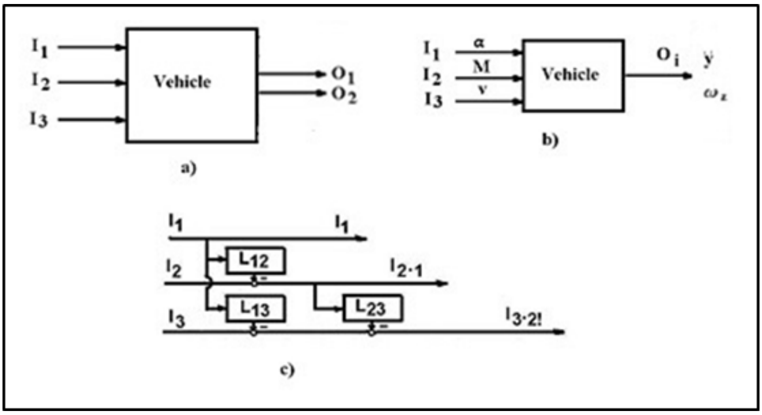

Figure 17 Scheme of a system with three input and two output sizes (legend: I1-I3 present input excitation values (α, M, v), and O1-O2 registered lateral accelerations and yaw (a_y, ω_z)

The spreading of the input quantities is done on the basis of the expression, Figure 17c [26-28]:

$$\begin{aligned} I_1 &= I_1 \\ I_{2.1} &= I_2 - L_{12} I_1 \\ I_{3.2!} &= I_3 - L_{13} I_1 - L_{23} I_{2.1} \end{aligned} \tag{1}$$

Expression (1) uses quantities according to Figure 17, and transfer functions between conjugate expressions defined by expression [26-28]:

$$L_{12} = \frac{I_2}{I_1} \qquad L_{13} = \frac{I_3}{I_1} \quad L_{23} = \frac{I_{3\cdot 1!}}{I_{2\cdot 1!}} \tag{2}$$

According to [26-28], the functions of partial coherences are defined by expression:

$$\gamma^2_{iQ(i1)!} = \frac{\left[S_{iQ(i-1)!}\right]^2}{S_{xx(i-1)!} S_{QQ(i-1)!}} \tag{3}$$

where are:

- $S_{iQ(i-1)}$ – cross-spectrum,
- $S_{xx(i-1)!}$, $S_{QQ(i-1)!}$ – appropriate auto-spectrum

In order to calculate the partial coherence functions, the Demparcoh program was used [29].

Using the mentioned program, the functions of partial coherences during rectilinear driving were calculated, shown in Figures 18 and 19.

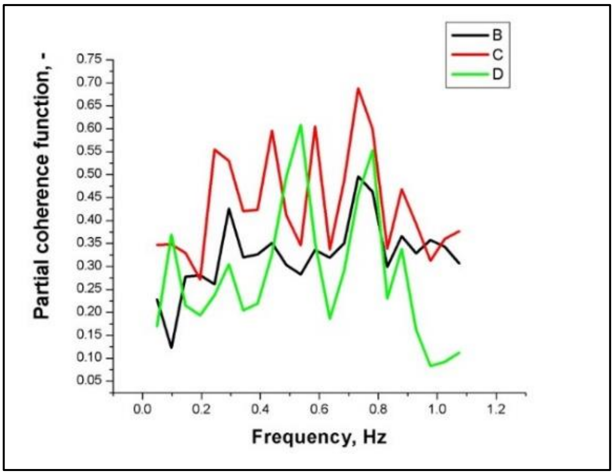

Figure 18 Partial coherence function: lateral acceleration – steering wheel angle(B), torque at steering wheel with the excluded influence of the steering wheel (C) and velocity with excluded influence of angle and torque at steering wheel (D), in rectilinear drive test

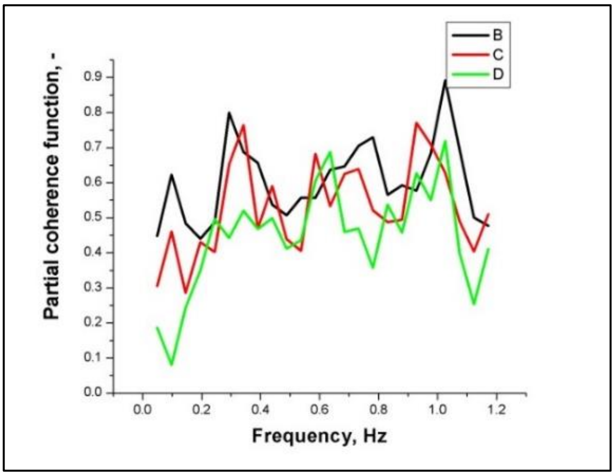

Figure 19 Partial coherence function: yaw – steering wheel angle (B), torque at steering wheel with excluded influence of steering wheel angle (C) and velocity with excluded influence of angle and torque at steering wheel (D), in rectilinear driving test

By analyzing the data from Figures 18-19, it can be determined that there is a statistical link between the registered kinematic parameters of the vehicle center of gravity movement and input excitations in the frequency range up to about 1.1 Hz. When it comes to lateral acceleration (Figure 18) in the area of the excitations largest amplitudes, the greatest impact has the torque on the steering wheel, and the least the vehicle velocity. Figure 19 shows that the steering angle has the greatest influence on the yaw and vehicle velocity has the smallest. It is noted that these effects are not unambiguous, especially above about 0.5 Hz, so it was considered expedient to analyze values that carry more information about the signal energy in the range up to about 1.1 Hz. The most practical value is RMS, which is calculated for all partial coherence functions and shown in Table 1.

Table 1 *Partial coherence functions in rectilinear driving test*

Measured value	*, -	**, -	***, -
Lateral acceleration, m/s^2	0.333	0.448	0.315
yaw, ^{o}/s	0.614	0.545	0.469

* - Steering wheel angle

**- Torque at steering wheel with excluded steering wheel angle

***-Vehicle velocity with excluded angle and torque at steering wheel

By analyzing the data from Table 1, it can be determined that all kinematic parameters of vehicle center of gravity movement are affected by controlled and partially controlled excitation. At the same time, the torque on the steering wheel has the greatest impact on lateral acceleration during rectilinear driving, and the vehicle velocity has the least. When analyzing the yaw, the angle of the steering wheel has the greatest influence, and the vehicle velocity has the least. For illustration, Figures 20 and 21 show the partial coherence functions of the vehicle during the DLC test.

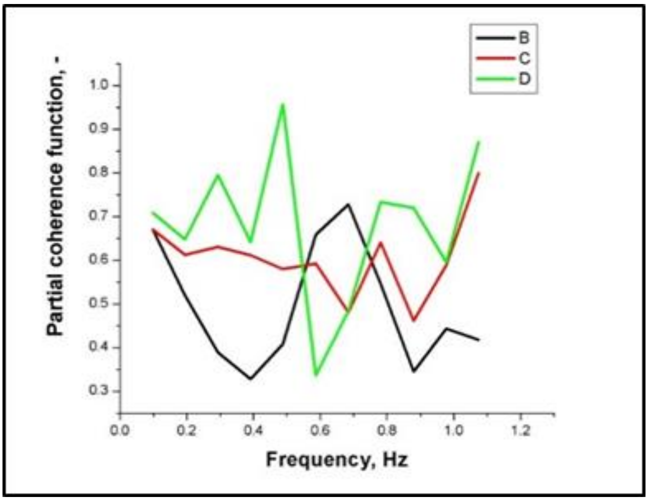

Figure 20 Partial coherence function: lateral acceleration – steering wheel angle (B), torque at steering wheel with excluded influence of steering wheel angle (C) and velocity with excluded influence of angle and torque at steering wheel (D) during DLC test

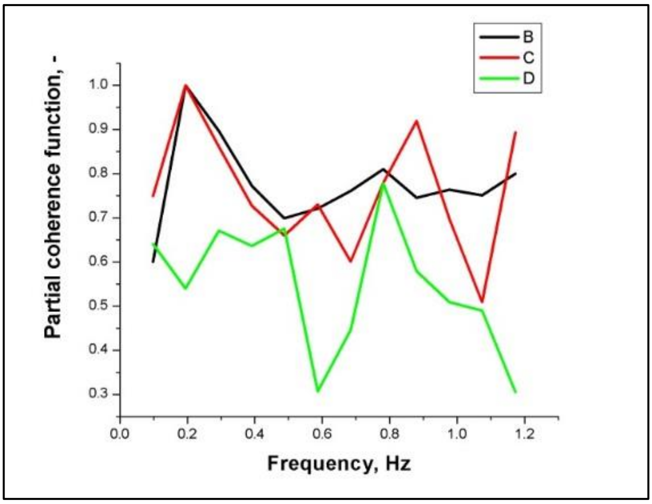

Figure 21 Partial coherence function: yaw – steering wheel angle (B) , torque at steering wheel with excluded influence of steering wheel angle (C) and velocity with excluded influence of angle and torque at steering wheel (D) during DLC test

The analysis of the calculated partial coherence functions shown in Figures 20 and 21, in the case of DLC test, shows that there is an influence of controlled and partially controlled excitations on the kinematic parameters of the vehicle center of gravity movement. Figure 20 shows the greatest influence of vehicle velocity on the lateral acceleration in the area of maximum excitation amplitudes, and the smallest steering wheel angle. When it comes to yaw during the DLC test, the steering wheel angle has an almost identical effect at the torque and the vehicle velocity has the lowest. In the regions higher than about 0.5 Hz, the effects are not so unambiguous, so it was considered expedient to calculate the effective values of the partial coherence functions and show them in Table 2.

***Table 2** Partial coherence functions during DLC test*

Measured value	*, -	**, -	***, -
Lateral acceleration, m/s^2	0.513	0.613	0.701
yaw, ^{o}/s	0.782	0.772	0.566

* - Steering wheel angle,
** - Torque at steering wheel with excluded influence of steering wheel angle,
*** - Vehicle velocity with excluded angle and torque at steering wheel.

By analyzing the data from Table 2, it can be determined that the vehicle velocity shows the greatest impact on lateral acceleration, and the smallest steering wheel angle. The steering wheel angle shows the greatest influence on the yaw during the DLC test and the smallest on the vehicle velocity. For illustration, Figures 22 and 23 show the partial coherence functions in the case of lateral acceleration and yaw, during the overtaking test.

Based on Figure 22, it can be argued that in the area of most interesting frequencies, up to about 0.5 Hz, during the overtaking test, the angle and torque at the steering wheel have the greatest impact on lateral acceleration, and vehicle velocity the least. When observing the yaw, the greatest influence has the torque at steering wheel and almost the same, the steering wheel angle and vehicle velocity has the least influence. For further analysis, it was considered expedient to calculate, as in previous cases, the effective values of the partial coherence functions, Table 3.

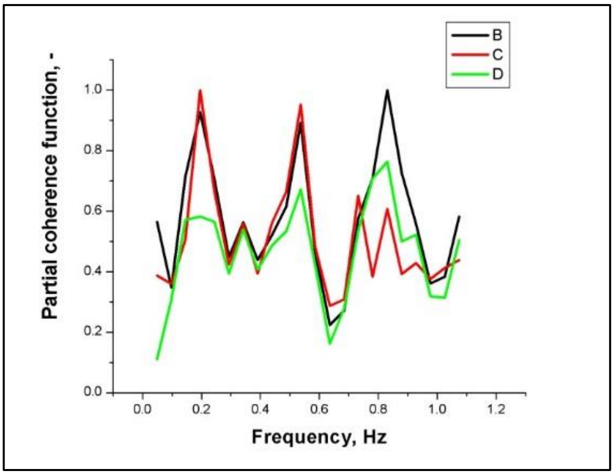

Figure 22 Partial coherence function: lateral acceleration – steering wheel angle (B), torque at steering wheel with excluded influence of steering wheel angle (C) and vehicle velocity with excluded influence of angle and torque at steering wheel (D) during overtaking test

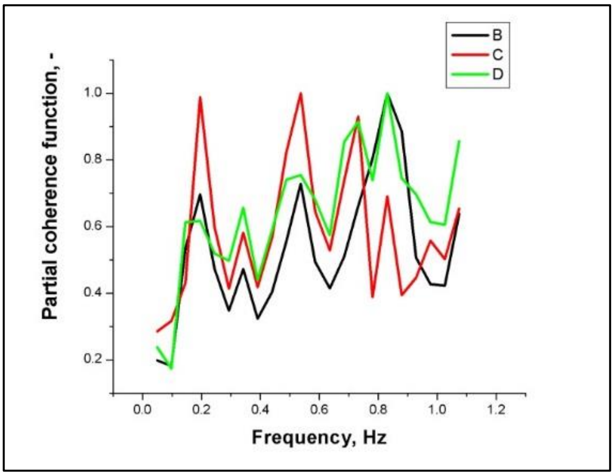

Figure 23 Partial coherence function: yaw – steering wheel angle (B), torque at steering wheel with excluded influence of steering wheel angle (C) and vehicle velocity with excluded influence of angle and torque at steering wheel (D) during overtaking test

Table 3 *Partial coherence functions during overtaking test*

Measured value	*, -	**, -	***, -
Lateral acceleration, m/s^2	0.607	0.543	0.491
yaw, ^{o}/s	0.568	0.620	0.670

* - Steering wheel angle;

** - Torque at steering wheel with excluded influence of the steering wheel angle;

*** - Vehicle velocity with excluded steering wheel angle and torque at steering wheel

By analyzing the data from Table 3, it can be determined that the steering wheel angle shows the greatest impact on lateral acceleration and the least vehicle velocity. The vehicle velocity has the greatest influence on the yaw, and the smallest steering wheel angle. Based on the previous analysis, it can be argued that this test also allows a good expression of the influence of controlled and partially controlled excitation on the parameters of vehicle handling. It was expected that there was no identical influence of the observed excitations in overtaking tests and DLC tests, which can be explained by nonlinearities in vehicle suspension systems [24].

As conclusion, the overtaking test can be used as the most suitable and the safest, during the research of truck behavior parameters on the road.

3. CONCLUSIONS

Based on the performed research, it can be concluded that there is an influence of controlled (angle and torque of the steering wheel) and partially controlled excitation (velocity) on the parameters of vehicle behaviour on the road.

The used methodology of data processing in the frequency domain made it possible to determine that the most pronounced values of the spectrum of excitation amplitudes (input quantities) are up to about 0.2 Hz. As there is a statistical link between the mentioned initiatives, it was considered expedient to use the method of "dissociation" based on partial coherence functions for further research.

The effects of the observed motives are not unambiguous in all tests. After comprehensive analyses, it can be argued that the rectilinear test does not cause sufficient impact on the parameters of truck behaviour on the road, and that the DLC tests and overtaking tests allow a good expression of the impact on these parameters. Therefore, overtaking tests and DLC test can be used as reliable tests, but due to simplicity and safety, the overtaking test is preferred.

REFERENCES

[1] Demić, M.: “Cybernetic system: Human-Vehicle-Environment “, Serbian Academy of Sciences and Art Research Centre and Kragujevac University (in Serbian, monograph): 2008.

[2] Lin, Y. et all.: “Artificial neural network modelling of driver handling behaviour in a driver-vehicle-environment system”, International Journal of Vehicle Design, 2005, Vol. 37, No 1, pp. 24-45.

[3] Radonjić, R.: “The identification of dynamic characteristics of motor vehicles”, Monograph, Mech. Eng. Faculty in Kragujevac (in Serbian), 1995.

[4] Gu, X., Yu, Q.: “Driver-vehicle-environment closed-loop simulation of handling and stability using fuzzy control theory”, Proceedings of 13th IAVSD Symposium, Chengdu, China, 1993, Vol. 10, pp. 172 ± 181.

[5] Lin, Y., Yu, Q.: “A study on driver model using neural network systems”, The Proceedings of the 12th ISTVS International Conference, Beijing, China, Oct. 7±11 1996, pp. 341 ± 348.

[6] Papntoniov, P. et all.: “ Review of driving performance parameters Critical for distracted driving Research”, Procedia, 25C, 2017, pp. 1801-1810.

[7] Hachaturov, A.A. et all.: “Dynamics of system: Road-Tire-Vehicle-Driver”, Mašinostrojenije, Moscow (in Russian), 1976.

[8] Fiala, E., Mensch und Fahrzeug, ATZ/MTZ Fachbuch, 2006.

[9] Hessburg, T., Tomizuka, M.: “Fuzzy logic control for lateral vehicle guidance“, Proceedings of the IEEE Conference on Control Applications, 1993, Vol. 2, pp.581±586.

[10] Viela, D. et all.: "Analytical Models Correlation for Vehicle Dynamic Handling Properties, December", Journal of the Brazilian Society of Mechanical Sciences and Engineering, 2011, Vol. 33, No. 4, pp. 437-444, DOI:10.1590/S1678-58782011000400007.

[11] Uys, P.E.: "Criteria for handling measurement", Journal of Theramechanics, 2006, Vol. 43, pp. 43-67.

[12] Panke, D.A, et all.: "Review on Handling Characteristics of Road Vehicles", Int. Journal of Engineering Research and Applications, 2014, Vol. 4, Issue 7 (Version 4), pp. 178-182, ISSN: 2248-9622.

[13] Abe, M., Manning, W.: "Vehicle handling Dynamics", Elsevier, 2009.

[14] Ellis, J. R.: "Vehicle Dynamics", Business Books, London, 1973.

[15] Genta, A.: "Motor Vehicle Dynamics – Modeling and Simulation", Singapore: World Scientific Publishing, 2003.

[16] Gillespie, T.: "Fundamentals of vehicle Dynamics", SAE, 1992.

[17] Milliken, W., Milliken, D.: "Race car dynamics", SAE, 1995.

[18] Mitschke, M.: "Dynamik der Kraftfahrzeuge", Springer Verlag, 1972.

[19] Rajamani, R.: "Vehicle Dynamics and Control", Springer Verlag, 2006.

[20] Preleov, V.VI.: "A fast method for measuring of the density of the road spectrum", Bulletin of the Moscow University, Mat. Mech, 1989, Number 6, pp. 74-76.

[21] Demić, M. et all.: "The Road Surface Profile Investigation Perspective", The 30' Session Modern technologies in XXI Century», Bucharest, Romania, CD, 2003, pp. 35-42.

[22] Demić, M.: "Dynamic excitation of vehicles", Institute for nuclear sciences Vinča – Centre for engines and vehicles, 2006.

[23] ISO 8608, Mechanical vibration – road surface profile – Reporting of measured data, 1995.

[24] Pacejka, H.B.: "Tyre and Vehicle Dynamics", Butterworth Heinemann, Elsevier Science, 2002.

[25] Cox, D.R. et all.: "The Theory of the Design of Experiments", Chapman and Hall/CRC, Boca Raton, London, New York, Washington, 2000.

[26] Bendat, J.S., Piersol, A.G.: "Random Data Analysis and Measurement Procedures", John Wiley and Sons, London, 2000.

[27] Bendat, J.S.: "Nonlinear Systems-Techniques and Applications", John Wiley and Sons, London, 1998.

[28] Bendat, J.S, Piersol, A.G.: "Engineering Applications of Correlation and Spectral Analysis", John Wiley and Sons, London, 1980.

[29] Demić, M.: Softwares- "Demparkoh", "Analsigdem", 2001, www.ptt.rs/korisnici/i/m/imizm034.

MOBILITY & VEHICLE MECHANICS

DOI: 10.24874/mvm.2022.48.01.02
UDC:629.3.016

THE ANALYSIS OF COMMERCIALLY AVAILABLE ELECTRIC CARS

Mladen Josijević [1], Dubravka Živković [2], Dušan Gordić [3], Davor Končalović [4], Vladimir Vukašinović[5]*

Received in April 2022 *Accepted in May 2022*

RESEARCH ARTICLE

ABSTRACT: This paper aims at providing an overview of commercially available electric cars at the global market, with the exception of China. 63 different models of electric cars are currently available, and for all models we have collected the data on price, battery capacity, efficiency, autonomy, acceleration, and maximum speed. We have calculated the charging costs per one charging session to batteries' full capacities and the charging costs per 100km, based on the average electricity price in Serbia. Technical and economic analysis is conducted for the models which are first classified into different categories based on their autonomy in order to ensure better understanding of cars' properties and their relative differences. The results obtained here can help prospective customers to choose the model of an electric car that meets their requirements and satisfies their need.

KEY WORDS: *electric cars, trend, market, characteristics*

[1]*Mladen Josijević, PhD, Assistant Professor, University of Kragujevac, Faculty of Engineering, Sestre Janjić 6, 34000 Kragujevac, Serbia, mladenjosijevic@gmail.com, https://orcid.org/0000-0001-9619-0897 (*Corresponding author)*

[2]*Dubravka Živković, PhD, Research Associate, University of Kragujevac, Institute for Information Technologies, Department of Technical-Technological Sciences, Jovana Cvijića bb, Kragujevac, dubravka@uni.kg.ac.rs, https://orcid.org/0000-0002-0266-456X*

[3]*Dušan Gordić, PhD, Full professor, University of Kragujevac, Faculty of Engineering, Sestre Janjić 6, 34000 Kragujevac, Serbia, gordic@kg.ac.rs, https://orcid.org/0000-0002-1058-5810*

[4]*Davor Končalović, PhD, Associate professor, University of Kragujevac, Faculty of Engineering, Sestre Janjić 6, 34000 Kragujevac, Serbia, davor.koncalovic@kg.ac.rs, konchalovic@gmail.com,* https://orcid.org/0000-0003-1207-2653

[5] *Vladimir Vukašinović, PhD, Assistant professor, University of Kragujevac, Faculty of Engineering, Sestre Janjić 6, 34000 Kragujevac, Serbia, vladimir.vukasinovic@kg.ac.rs https://orcid.org/0000-0001-6489-2632*

ANALIZA KOMERCIJALNO DOSTUPNIH MODELA ELEKTRIČNIH AUTOMOBILA

REZIME: U radu je izvršen pregled komercijalno dostupnih modela električnih automobila na svetskom tržištu, izuzev Kineskog tržišta. Utvrđeno je da je trenutno dostupno 63 različitih modela elektricnih automobila. Za sve modele prikupljeni su podaci o cenovnom rangu, dostupnim kapacitetima baterija, efikasnosti, autonomiji, ubrzanju i maksimalnoj brzini. Izračunati su troškovi punjenja do maksimalnog kapaciteta kao i troškovi za pređenih 100km, a na osnovu prosečne cene električne energije u Srbiji. Izvršena je tehno-ekonomska analiza svih dostupnih modela koji su radi lakšeg razumevanja njihovih svojstava i razlika prvo klasifikovani u nekoliko kategorija na osnovu autonomije. Rezultati dobijeni ovom analizom mogu da pomognu potencijalnim kupcima električnih automobila pri odabiru modela koji zadovoljava njihove zahteve i potrebe..

KLJUČNE REČI: *električni automobil, trend, tržište, karakteristike*

THE ANALYSIS OF COMMERCIALLY AVAILABLE ELECTRIC CARS

Mladen Josijević, Dubravka Živković, Dušan Gordić, Davor Končalović

INTRODUCTION

According to Eurostat data, transport accounted for 30.5% in the total consumption of final energy in 27 countries of the European Union (EU-27) in 2018 [1]. The same year, the energy consumption in the world reached 2808 megatonnes of oil equivalent (Mtoe), with oil products accounting for 92% of that amount. In addition, 49.2% of the oil was consumed within the road transport sector [2]. According to [3], the transport sector is also a major emitter of air pollutants and greenhouse gas (GHG) emissions because of its dependence on fossil fuel. In 2017, transport accounted for 24% in the global CO_2 emissions. In 8 gigatonnes of CO_2 emitted by transport globally, road transport participated with 74% [2]. Based on the aforementioned data, it is not surprising that The United Nations Framework Convention on Climate Change has highlighted the critical role that transport plays in climate changes.

Owing to the environmental concerns, the reduced consumption of fossil fuels, and the fluctuations in oil prices, electric vehicles (EVs) have gained popularity in developed countries. Several countries, such as China, the UK, the EU countries, and the U.S., have promoted the use of EVs during the last decade by providing supports from the local and national bodies to consumers [4]. The replacement of conventional vehicles, powered by gasoline and diesel, with zero- and low-emission vehicles has been widely accepted as a solution to environmental and energy-waste issues. Battery electric cars reduce air pollutant emissions, such NOx, NO2, and particulate matter [3]. However, their greatest benefit of EVs is the low emission rate of CO2, together with higher acceleration and lower noise emissions [5-7]. One-step closer to cleaner transport was also the declaration of electro-mobility signed by 44 countries, 5 regions/cities and 32 international NGOs [3].

The market diffusion has been facilitated by constant efforts to increase the number and availability of charging stations, to improve government regulations on carbon emissions, and provide subsidies and other incentives (i.e. free charging, free access to car parks or entry into environmental zones) [8]. The factors that should drive the growth of EVs include high decreases in battery prices, improvements in infrastructure and raised awareness about environmental issues in consumers [5]. However, the response by consumers is still below expected levels. The lower acceptability of electric cars (ECs) by end consumers has been attributed to national and local policy frameworks, insufficient infrastructure development, existent vehicle technology, and consumer perceptions [9]. The following factors have also been found to influence the decision to buy ECs: battery size, availability of charging stations, driving range, cost of ownership, and prices of operation and maintenance [10, 11]. Over the years, many reviews on the abundant literature dedicated to EVs have become available [12-15]. They strive to analyze and explain the factors which impact the adoption of “a new technology – electric cars.” Among the technical attributes of ECs, the driving ranges and battery degradation have received more attention while acceleration and maximum speeds have been seen as less problematic.

The market of electric cars has been growing exponentially, including the number of manufacturers expanding their supply of models that are fully electricity-driven. With the diversity of models already available, a new challenge for customers is now how to choose the model that they will purchase. These insecurities may hinder faster decisions to buy an electric car so it is crucial to provide more guidance to end customers. The current databases of all-electric cars usually include the following technical properties and economic indicators: minimum prices (for the basic packages of equipment), maximum prices (for the best offered packages of additional equipment), battery sizes (kWh), battery efficiencies (km/kWh), ranges (mileage per one charging session), acceleration from 0 – 100km, and maximum speeds that a model can develop. Such presentations may be confusing for potential customers and result in undesirable procrastination. Obviously, a price is not a guarantee of performance. Cars with similar characteristics can differ in prices significantly. On the other hand, cheaper solutions may not be efficient enough as some more expensive options, so in a long run, customers may eventually end up saving by buying pricier models. In addition, a battery size does not necessarily mean better range (mileage per one charging session). More efficient cars may secure better range even though they have lower battery capacities.

These new challenges that customers are currently facing served as a motivation for this paper. Four categories of all-electric cars are analyzed here: city cars, family cars, long-drive cars and SUVs. This research aims at collecting the data on commercially available models of all-electric cars in order to create a comprehensive systematic review of their most crucial technical and economic properties. The focus is on their minimum price, battery capacities, charging powers, efficiency and range. Efficiency and range are recognized as the most relevant properties in the current literature. We follow this line of thought. However, we are all aware that theory and practice frequently clash. In practice, most commonly the most relevant factor is customers' budget. In other words, no matter how energy-efficient and environment-friendly a car is, we will not see it on our streets as we wish if it is unaffordable. Price is not the only economic indicator that should be taken into account. Since the charging infrastructure is underdeveloped, we shall assume that most customers will rely on their household electricity sources for re-charging a vehicle. Thus, the costs of charging a battery are among the most relevant factors for prospective customers. Based on the collected data on battery capacities, charging powers and model efficiencies, we calculated the charging costs for electricity used to charge a battery to its full capacity and charging costs for used electricity per 100km, based on the adopted average price of electricity in Serbia. These indicators may be also crucial if cheaper models prove to be inefficient and considerably more expensive to re-charge.

1. TRENDS AND DEVELOPMENTS OF ELECTRIC CARS

1.1 Electric cars architecture

Several types of battery-equipped cars have been introduced in the last decade or so, which are mainly classified into four categories: All-electric cars (AECs), Hybrid Electric cars (HECs), Plug-in hybrid electric cars (PHECs), and fuel cell-based EVs. The latter category has lesser emissions and higher efficiency, but high hydrogen production costs, underdeveloped infrastructure and lower commercial availability are a serious obstacle. The paper will focus solely on all-electric cars which use batteries as their sole energy source.
AECs use battery packs and electric motors for traction purposes (Figure 1. (c)). AECs have several benefits over other cars (i.e. conventional ICE cars, HECs, and PHECs), including: smooth operation, higher efficiency, absence of noise pollution, and minimal local GHG emissions. The efficiency of AECs has been evaluated at 60 – 70%, which is substantially higher than 15 – 18%, which is a value range attributed to ICE-based cars [16].

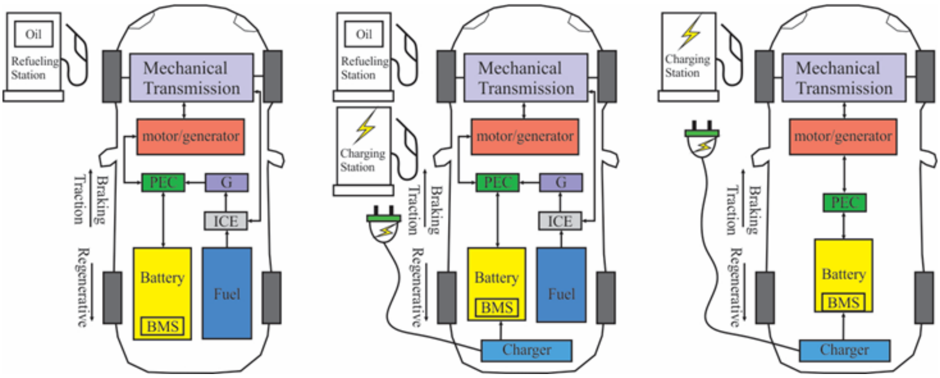

Note: PEC-Power electronic converter, BMS-Battery management system, ICE Internal combustion engine, G-generator

Figure 1 Power train architectures of ECs: (a) Hybrid electric car, (b) Plug-in hybrid electric car, and (c) Full-electric car

1.2 Trends in electric cars

The car market has recorded a huge expansion during the last few years. The growing concerns about the environment, reduction of fossil fuels and fluctuating prices of oils instigated the increases in EC use especially in developed countries. 130,000 electric cars were sold in only one week of 2021. The same amount was sold during the whole year of 2012. The growth has been very intensive during the last three years, despite the fact that the global pandemic has had a negative impact on car sales in general. Namely, the crisis has had no impact on the EC market. In 2020, the total car market reduced, and during the same year over 3 million ECs were sold (accounting for 4.1% in the global car market).
Even though these improvements are considerable, and the EC sales have grown significantly, their ratio in the total car sale is still relatively low. For instance, ECs participated with 2.5% in 2019, and 9% in 2021. Actually, the number of sold ECs doubled in 2021 with respect to 2020 and it finally reached the number of 6.6 million sold cars. The estimated number of electric cars on the road across the world is now approximately 16 million. They consume about 30TWh of electricity. Just for a comparison, it must be noted here that the annual consumption of electricity in Serbia is about 35TWh, in Montenegro 3.8TWh, in Croatia 15TWh, and in Bulgaria 37TWh [17]. The figure 2 shows the sale trends for electric cars since 2010.

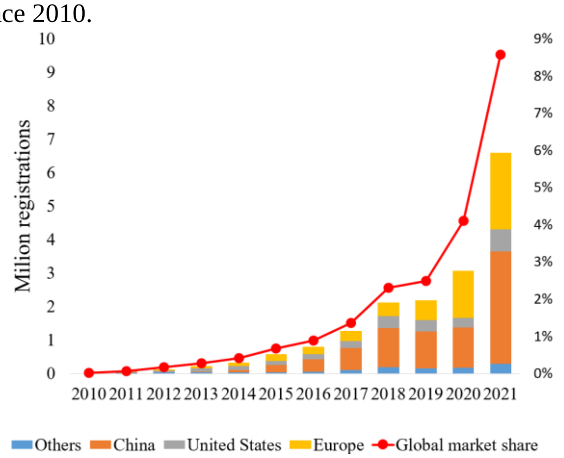

Figure 2 Global sales and sales market share of electric cars, 2010-2021 [18]

As the Figure 2 demonstrates, China was a global leader on the market of electric cars in 2021. The sales in this country increased by more than three times in 2021 (3.4 million cars) in comparison to 2020 (about one million). In China only, more ECs were sold in 2021 than in the entire world in 2020. The ratio of sold ECs on the global market leaped from 7.2% in January to 20% in December. With these trends, China has good chances of reaching the Government's goal – 20% for the whole 2025. The sales are also expected to increase during the following year. The sales of electric cars in Europe are also in expansion. The increase of 70% has been recorded in Europe in a year (2021 versus 2020). In 2021, 2.3 million electric cars entered the roads in Europe. The surge in EC sales in Europe during 2021 was at least partially initiated by new standards on CO_2 emissions. In addition, the purchase subsidies were also increased and expanded in most major European markets. Overall, ECs accounted for 17% of the total car sales in Europe in 2021. However, there are tremendous diversities across the different markets. For instance, more than 30% of sold cars in Germany during the last quarter of 2021 were ECs. Still, Norway appears to be a European leader since 72% of all sold cars were ECs. Sweden and the Netherlands recorded 45% and 30% respectively, during 2021.

In the United States, the sales of electric cars doubled in 2021 after a period of stagnation and a decrease in 2019 and 2020. Over one million electric cars were sold in 2021, but they still account for only 4.5% in the total car sales, which is still a relatively low share.

It should be probably noted here that both governments and car industry faced some challenges during 2021. Tight supplies of components and increased prices of bulk materials now place supply concerns as the main priority. Taking into consideration that China, Europe and the U.S. account for only 60% of the global car market and use above 90% of electric cars, we can conclude that the whole concept of electric vehicles is extremely underdeveloped in the remaining parts of the world. For instance, in Brazil and India the share of electric cars in total car sales is below 2%. These values are unacceptably low. The reasons for this lag mainly include: the lack of institutional support and subsidies. These measures should be intensified in the future [19].

The truth is that government policies are the key driving force for global electric car markets. Many countries have introduced several different incentives for buyers and production companies in order to promote the use of ECs over fossil-fuel vehicles. In Europe, the market has been growing rapidly for the last few years. The main contributors are the Netherlands, France, Germany, and the United Kingdom. The benefits for buyers include a tax reduction or a tax exemption. These are generally one-time or annually-based taxes that are mostly paid while purchasing a vehicle. Other benefits for customers include free use or discounts on using parking facilities, free charging at public charging infrastructures, etc. The Netherlands, for instance, offers an exemption to AECs from paying the registration tax and the road taxes are completely waived. AECs can use other benefits here as well, such as: free parking, 100% tax benefits (excluding VAT), and waiver in registration taxes [16, 20, 21].

Still, the supply on the market has grown exponentially. With the growing supply and the surge of new models that are now available at the market, new challenges for customers entered the scene. Namely, after making a decision to replace their old car with an electric solution, they now must make another big decision – which model to choose in this vast variety. While even laymen are informed enough what to look for in a conventional car, electric cars have remained a mystery to ordinary customers who do not fully understand which properties are the most relevant. In order to make an informed decision which electric car to purchase, it is necessary for customers to have a comprehensive summary of what is currently offered on the market and which options are the most appropriate for their own context – budget, operational (i.e. charging) costs based on the electricity price in their country, etc. In the Serbian context, as in many developing countries, the low purchasing power can be a serious obstacle. On the other hand, Serbia is has the highest production of electricity from coal per capita in whole Europe. Thus, it is quite possible that all-electric cars which require greater quantities of energy will fail to fulfill their main purpose – to be eco-friendly.

2. METHODOLOGY OF COLLECTING AND SYSTEMATING DATA ON ELECTRIC CARS

The significance of increasing the participation of ECs on our roads and the failure to see the new technology embraced by consumers motivated us to conduct an analysis of commercially available all-electric cars. Its main contribution will be to facilitate the decision-making process by systematizing the data on commercially available models of electric cars worldwide and providing a comprehensive overview. The data are collected from the relevant webpage which updates the data on commercially available models of electric cars and their technical and economical features daily [22]. We focused on car prices (minimum only), battery capacities, car efficiencies, maximum charging powers and range. We must highlight that the prices presented here may differ from the prices given on other websites. However, we shall adopt the values provided by the same source from which we obtained the data about model properties. Some data about some models are not provided on the selected website. Even though we could obtain them from other sources, we decided not to do so in order to avoid the inclusion of data from multiple different sources and potential confusion. Finally, some models have two options for batteries and with more capacity there comes a higher range. Here we shall focus only on smaller batteries and thus smaller ranges.

Based on the collected data on battery capacities, charging powers and model efficiencies, we calculated the charging costs to maximum capacity for each model (FCC in Equation 1). We have also calculated the specific costs for 100km (SC in Equation 2).

$$FCC = BS_a \cdot EC_a \tag{1}$$

where:

BS_a

EC_a -[kWh] - Battery size (average)

-[€/kWh] – Electricity price (average)

$$SC = EEC \cdot EC_a \tag{2}$$

where:

EEC - [kWh/km] – Electric car efficiency

The mean price of electricity in Serbia equals 0.08 €/kWh [23]. Taking into consideration that these cars are mostly charged during night (lower prices for used electricity in Serbia), the prices for charging a car should be lower than this average. We shall neglect this discrepancy because some factors may simultaneously make the real price higher than this mean value. Namely, the average annual mileage in Serbia is about 10,000 kilometers [24]. The average electric car whose battery capacity is about 60kWh could pass 250km with a full battery. This means that an average car should be re-charged about 3 to 4 times a month (about 200kWh of electricity). Taking into consideration that the average consumption of electricity in a Serbian household is 470kWh, the total consumption with an electric car would increase by more than 40%. It is reasonable to expect that this increase would result in exceeding the *zone* limits. Namely, the Serbian tariff-charging system sets the zone limits and a kWh of used electricity in a higher zone is pricier than one kWh which is consumed in a lower one. In addition, due to high investments for purchasing electric cars, it is reasonable to expect that these cars would be primarily attractive to the richer subpopulation. They are also known to generally use more electricity in their households (higher charging zones) so the average value for electricity is significantly higher than the average for the whole Serbian population. For these reasons, we found it even more reasonable to increase the value of average electricity price to 0.09€/kWh.

Just for illustration purposes, the paper will compare the ranges per the same amount of money which associates charging costs and ranges per one re-charge. We find these examples less abstract. They are thus easier to understand, even for laymen. The adopted average price of electricity is the same for all cars, and the costs of re-charging session are calculated based on their battery size and car efficiency. When these costs are related to cars' ranges, all most relevant properties and economic indicators are included in their unique interaction.

3. RESULTS AND DISCUSSION

According to the data base retrieved from the selected source, about 63 models of all-electric cars are currently commercially available. In addition, there are plenty more models that are not available on all continents and, as such, they are excluded from our analysis. For instance, there are a few dozen models produced by Chinese manufacturers that are available only in China and/or in the neighboring countries.

Our analysis focuses on four categories of all-electric cars: city cars (C), family cars (F), long-drive cars (LD) and SUVs. Long-drive cars are a special category in that they include all cars from the previous three groups whose batteries allow a car to pass 300km or more after one charging session. Actually, there are no strict boundaries between these categories so the same car is classified in two or more groups simultaneously:

Table 1 *Overview of models based on their category*

Category	C	F	LD	SUV	C + F	C + LD	C + SUV	
No. of models	28	7	3	4	6	2	2	
Category	F + LD	F+ SUV	LD + SUV	C + F + LD	C + F + SUV	C + LD + SUV	F + LD + SUV	ALL 4
No. of models	12	4	2	6	3	3	14	3

Since it is pointless to use this classification due to numerous overlaps between the classes, the models will be classified here according to their range. Range is generally accepted as one of the most important properties, especially because the charging infrastructure is underdeveloped to the extent that it is highly probable that vast majority of customers will predominantly depend on household electricity sources for charging their vehicles, especially in developing countries, such as Serbia. The models are classified here based on their range into five categories: (1) less than 200km, (2) 200 – 300km, (3) 300 – 400km, (4) 400 – 500km, and (5) more than 500km.

Range: less than 200km

Only four cars have a mean range lesser than 200km which most customers may find unfavorable: Citroen Ami (71km), Renault Twitzy (90km), Smart EQ Fortwo (134km), and Microlino (162km). They are all classified as city cars and their prices range from €5,000 (Citroen Ami) to €19,150 (Smart EQ Fortwo). Renault Twitzy currently costs about €11,000, and Microlino is about €12,000. Despite the attractive price, the top speed that these cars can develop is another setback. Namely, Citroen Ami and Renault Twitzy can reportedly go 48km/h and 80km/h, respectively. The top speed is not reported for Macroline, so Smart EQ Fortwo is the only car from this low-range category whose speed exceeds 100km/h (130km/h). In other words, these cars are literally designed for city driving. Since they may be unattractive even for customers who need car for this sole purpose, we will exclude them from the further analysis, especially because there are options that are not significantly pricier that Smart EQ Fortwo, but offer better performances.

Range: 200 – 300km

The lowest acceptable range (from 200km to 300km) is found in sixteen models. The following table summarizes their technical properties and economic indicators.

As can be seen from the table above, most models from this category are classified as city cars (12 models), and/or as family cars (11 models), while there are only five models labeled as SUVs.

The prices range from €11,407 (Volkswagen e-UP!) to €41,264 (Honda e). By far the cheapest option is Volkswagen e-UP!, and the next cheapest candidate within this range is Dacia Spring (€21,614). Nissan e-NV200, SEAT Mi Electric, Fiat 500e, and Renault Kangoo Ze cost from €24,021 to €29,014, respectively. Fiat appears to be the most lucrative option within this price range in terms of charging costs (€2.6 per one charging session and €1.8 per 100 km). However, if we combine charging costs with ranges, we can conclude that SEAT Mi Electric and Dacia Spring can pass higher distances for the same amount of money.

Renault Kangoo ZE is not much cheaper than the models from the following price range. There are seven models that cost between about €31,000 and 34,000. MG ZS V stands out in terms of its speed (262km/h). With all other models the speed is fairly similar (about 150 – 167km/h). MINI Electric, Hyundai Kona Electric, and Vauxhall Vivaro-e are the most efficient, and the highest ranges are reported for Kia eNiro, Hyundai Kona Electric, and Nissan Leaf. The highest charging costs per charging session are calculated for MG ZS V and Vauxhall Vivaro-e (€9.0 and €6.3). The results indicate that Hyndai Kona Electric and Kia eNiro can pass the longest distances with the same amount of money. MG ZS V and Vauxhall Vivaro-e are significantly lagging behind. For nine euros, MGZS V can be charged once and pass about 290km. Both Hyndai Kona Electric and Kia eNiro can pass about 826km for the same amount of money. These results indicate that efficiency and range are the most important properties and that they can provide a clearer image on cars' performances when combined with charging costs. These should never be observed in isolation. For instance, MINI Electric has the best efficiency (8.8km/kWh), but its range is lower by 233km than those found in Hyndai Kona Electric and Kia eNiro. As a result, it can pass just a half of the distance that the other two cars can reach for the same amount of money.

Citroen ë-Space Tourer, BMW i3 and Honda are significantly pricier (€37,196, €40,592, and €41,264, respectively). The most efficient option is BMW i3 which also has the highest range, top speed, and charging price per session. Even though it can pass larger distances for the same amount of money than other two models, we must note that it cannot surpass Hyndai Kona Electric and Kia eNiro in this aspect because both its range and efficiency are lower.

***Table 2** Technical properties and economic indicators (range: 200 – 300km)*

Model	Category	Min. price [€]	Battery size [kWh]	Efficiency [km/ kWh]	Range [km]	Accelerating 0-100 km/h [s]	Top speed [km/h]	Charging costs per charge [€]	[€/100km]
Volkswagen e-UP!	C	11,407	32.3	8.42	261	12.32	130	2.91	1.07
Dacia Spring	C, SUV	21,614	27	8.40	225	-	-	2.43	1.07
Nissan e-NV200	F	24,021	40	5.39	200	14.5	122	3.60	1.67
SEAT Mii Electric	C, F	25,576	32.3	8.42	272	12.7	130	2.91	1.07
Fiat 500e	C, F	26,411	24	7.63	185	-	150	2.16	1.18
Renault Kangoo ZE	C, F	29,014	33	7.11	230	21.0	130	2.97	1.27
MG ZS V	C, F, SUV	31,411	44.5	5.89	262	7.56	261	9.0	1.48
Nissan Leaf	C, F	32,415	40	6.20	270	7.6	156	3.60	1.45
MINI Electric	C, F	32,421	32.6	8.08	233	7.56	150	2.93	1.11
Mazda MX-30	C, F, SUV	32,475	35.5	6.76	200	10.0	150	3.20	1.33
Kia eNiro	F, SUV	32,845	39	7.10	290	7.77	167	3.51	1.27
Vauxhall Vivaro-e	F	33,179	50	4.84	232	-	-	6.3	1.5
Hyundai Kona Electric	C, F, SUV	34,762	39	7.55	290	10.05	167	3.51	1.19
Citroen ë-SpaceTourer	F	37,196	50	5.12	219	-	-	4.5	1.25
BMW i3	C	40,592	42	6.63	278	7.15	159	3.78	1.36
Honda e	C	41,264	35.5	5.66	220	8.60	145	3.20	1.59

Range: 300 – 400km

For sixteen models the range varies from 300km to 400km. Their technical properties and economic indicators are presented in Table 3.

The models with the desired range vary greatly in price and other characteristics. The cheapest model is Vauxhall Mokka (€30,895), and the most expensive is Mercedes EQV (€80,840), followed by Mercedes EQC (€78,915) and Audi e-tron (€72,767).

Table 3 *Technical properties and economic indicators (range: 300 – 400km)*

Model	**Category**	**Min. price [€]**	**Battery size [kWh]**	**Efficiency [km/ kWh]**	**Range [km]**	**Accelerating 0-100 km/h [s]**	**Top speed [km/h]**	**Charging costs per charge [€]**	**[€/100km]**
Vauxhall Mokka	All four	30,895	50	7.19	336	-	-	4.5	1.3
Vauxhall Corsa-e	C, F, LD	32,565	50	7.47	336	-	-	4.5	1.2
Citroen e-C4	C, F, LD	34,216	50	7.76	349	9.3	150	4.50	1.16
Renault Zoe	C	34,336	52	7.4	383	9.84	-	8.10	1.73
SsangYong Korando e-Motion	F, SUV	36,617	61.5	-	338	-	249	9.0	1.46
Peugeot e2008	All four	41,102	50	6.82	332	9.3	150	4.50	1.32
Volkswagen ID.4	F, LD, SUV	42,021	52	6.49	340	6.4	180	4.7	1.4
DS3 Crossback E-Tense	C, SUV	44,308	50	7.02	315	9.32	150	4.50	1.28
Hyundai IONIQ Electric	C, F	44,933	38	8.22	312	5.4	150	3.51	1.39
Lexus UX3003	F, SUV	50,126	53.3	5.70	315	7.77	259	6.97	1.32
Nissan Ariya	LD, SUV	50,246	63	5.79	359	5.28	-	4.5	1.25
Audi Q4 e-tron	F, SUV	50,222	52	6.6	322	6.4	130	2.91	1.07
Tesla Model Y	F, LD, SUV	66,030	55	6.76	370	3.6	-	4.5	1.25
Audi e-tron	All four	72,767	71	5.13	300	3.75	209	6.4	1.8
Mercedes EQC	C, LD, SUV	78,915	80	4.65	372	5.28	180	7.20	1.94
Mercedes EQV	F, LD	80,840	90	3.77	340	-	259	6.39	2.26

Ssang Yong Korando e-Motion (249km/h) and Lexus UX3003 and Mercedes EQV (259km/h both) stand out in terms of top speed. Tesla and Audi e-tron have the best acceleration. The highest efficiencies are reported for Hyundai IONIQ Electric, Citroen e-C4 and Vauxal Corsa (more than 7km per kWh) while the lowest efficiencies are found in Mercedes EQV, Mercedes EQC, and Audi e-tron. Renault Zoe, Mercedes EQC, and Tesla Model Y have the largest ranges, while the opposite is the case with Audi e-tron, Hyundai IONIQ Electric, Lexus UX3003, and DS3 Crossback E-Tense. When charging costs are taken into consideration, we can see that Audi Q4 e-tron, Hyundai IONIQ Electric, and Tesla Model Y can pass the largest distances for the same amount of money. This once again shows that neither highest efficiencies nor highest ranges are a guarantee that a car has the best performances. These two properties must be observed in their unique interaction. The results also show that speed adds the price, but impacts the total performance quite unfavorably. Two fastest cars, Lexus while Mercedes EQV, have high charging costs and they can pass less than a half of the distance that Audi Q4 can for the same amount of money. Lexus is more efficient than Audi Q4 e-tron and Mercedes EQV has a higher range. Still, the model with a better combination of these two properties appears to be the most acceptable solution if we observe the models from this perspective.

Within the lower price range (€30,895 to €36,617), the most favorable interaction between efficiency and range is found in Citroen e-C4. After Hyundai IONIQ Electric, this is the second most efficient car in this category. This Citroen’s solution is cheaper by €10.000 than Hyundai’s IONIQ Electric, and as such, it is more affordable and will probably be perceived as more attractive option.

Range: 400 – 500km

According to the selected database, 18 models have a range from 402 to 499km per one full charge. This classifies them all as long-drive cars. Pininfarina Battista and Rimac Nevera are excluded from further analysis because they are not serially produced and their prices surpass 2 million euros. The technical properties and economic indicators are presented in Table 4.

Only two models within the selected ranges are non-SUVs: Volkswagen ID.3 and Tesla Model 3 (ordered based on their price). The price range for this category ranges from €33,105 to €51,621. The cheapest cars are MG 5EV and Renault Megane E-tech. The priciest cars in this category are Ford Mustang Mach-E, Jaguar I-Pace and BMW iX. The lowest battery capacities are reported for Tesla Model 3, Volkswagen ID.3, and Skoda EnyaqiaV, while the opposite is the case with Jaguar I-Pace, BMW iX3, and Volvo XC40 Recharge. The best efficiency is recorded for Tesla Model 3, Skoda EnyaqiV, and Hyndai IONIQ5. Jaguar I-Pace, BMW iX, and BMW iX3 are at the bottom of the list in terms of their efficiency. Volkswagen, Hyundai, Renault and Jaguare have the best ranges. The lowest ranges are reported for Ford Mustang, MG 5EV, and Skoda. MG 5EV, Tesla Model 3, Mercedes EQA, and Renault have significantly higher top speeds than the other models in this category. When costs needed for one re-charging are taken into consideration, the best results are found for Ford Mustang Mach-E, Jaguar I-Pace, and BMW iX. The opposite is the case with Tesla Model X and MG 5EV which stand out as the most extreme cases. For prospective customers it may be relevant to know that with the same amount of money the smallest distances can be passed with MG 5EV, Skoda EnyaquiV, Ford Mustang, and Volvo. The largest distances for the same amount of money can be passed with Ford Mustang, Jaguar I-Pace, and BMW iX. Within that price range, Ford Mustang has the best efficiency. Within the lower price range (€50,371 to €59,978), the best interaction of efficiency and range is exhibited by Tesla Model 3 which has both the highest efficiency and the highest range, and the lowest charging costs. Volkswagen ID.3, Skoda Enyaqi V, and Hyndai IONIQ 5 currently cost from €40,148 to €44,933. The biggest battery capacity is recorded for Hyundai (72.6kWh) while Skoda and Volkswagen have the batteries with the same capacity (58kWh). The highest efficiency is reported for Volkswagen, Skoda, and then Hyndai. Skoda has the highest costs per charging session (€8.1), as compared to Hyundai (€6.53) and Volkswagen ID.3 (€5.22). For the same amount of money, Hyndai can pass the largest distances even though its efficiency is the lowest since it has the best range (480km versus 425 and 412km).

Table 4 *Technical properties and economic indicators (range: 400 – 500km)*

Model	Category	Min. price [€]	Battery size [kWh]	Efficiency [km/ kWh]	Range [km]	Accelerating 0-100 km/h [s]	Top speed [km/h]	Charging costs per charge [€]	[€/100km]
MG 5EV	C, F, SUV	33,015	61	6.55	402	7.56	261	9.0	1.48
Renault Megane E-Tech	F, LD, SUV	37,224	60	0.0	470	7.46	209	6.39	1.75
Volkswagen ID.3	F, LD	40,148	58	7.02	425	9.9	161	5.22	1.28
Skoda EnyaqiV	F, LD, SUV	41,439	58	6.95	412	8.7	-	8.1	2.39
Hyundai IONIQ 5	F, LD, SUV	44,933	72.6	6.60	480	5.4	185	6.53	1.36
Toyota bZ4X	L, LD, SUV	50,372	71.4	6.28	451	7.1	159	6.43	1.43
Ford Mustang Mach E GT	LD, SUV	51,069	75	6.10	401	5.3	180	6.75	1.5
Tesla Model 3	C, F, LD	51,621	55	7.72	430	3.2	261	4.95	1.17
Mercedes EQA	F, LD, SUV	53.428	70	6.00	420	-	-	6.3	1.5
Volvo XC40 Recharge	F, SUV	59,978	78	5.34	417	5.1	180	7.02	1.68
Mercedes EQB	F, LD, SUV	61,239	66.5	6.29	418	6.42	241	6.75	1.33
Volkswagen ID.5 GTW	F, LD, SUV	66,444	77	6.4	496	6.42	-	6.93	1.4
BMW iX3	F, LD, SUV	70,665	80	5.73	459	7.0	185	5.49	1.37
Ford Mustang	F, LD, SUV	78,146	75	6.1	401	-	150	2.16	1.18

Mach-E									
Jaguar I-Pace	F, LD, SUV	78,284	90	5.21	470	4.7	166	3.42	1.09
BMW iX	F, LD, SUV	83,940	71	5.49	425	6.32	150	4.5	1.21

Range: more than 500km

According to the selected database, nine cars have a range higher than 500km (Table 5). The price range goes from €49,166 (KIA EV6) to €120,077 (Lucid Air).

Table 5 *Technical properties and economic indicators of models whose range is above 500km*

Model	**Category**	**Min. price [€]**	**Battery size [kWh]**	**Efficiency [km/ kWh]**	**Range [km]**	**Accelerating 0-100 km/h [s]**	**Top speed [km/h]**	**Charging costs per charge [€]**	**[€/100km]**
Kia EV6	F, SUV	49,166	77.4	6.82	528	3.66	159	5.22	1.29
Volkswagen ID. Buzz	F	60,039	77	-	550	-	-	6.39	1.64
BMW i4	F, LD	62,326	80	7.29	591	4.0	224	7.20	1.23
Toyota Mirai	F, LD	72,046	-	-	805	9.5	180	4.68	1.39
Mercedes EQE	F, LD	84,054	90	-	660	-	209	6.39	1.75
Tesla Model S	F, LD	96,038	100	6.10	591	2.4	-	10.8	2.17
Tesla Model X	All 4	105,644	100	6.18	560	4.56	150	3.2	1.33
Mercedes EQS	F, LD	109,264	108	7.15	771	-	-	6.39	1.64
Lucid Air	F, LD	120,077	90	-	660	3.1	-	4.98	1.58

The differences in prices in models with the selected range (>500km) are huge. The cheapest model is Kia EV6. The most expensive are Tesla Model X, Mercedes EQS, and Lucid Air. The most expensive car is about 2.4 times pricier than the cheapest one. The battery capacity is the worst in KIA EV6, Volkswagen ID. Buzz, and BMW i4 (77kWh, 77kWh, and 80kWh, respectively). The best battery capacity is found in Tesla Model S, Tesla Model X, and Mercedes EQS (100kWh, 100kWh, and 108kWh, respectively). Not all values for efficiencies are reported in the selected source. Based on those that are documented, BMW i4 and Mercedes EQS have the best efficiencies (7.9km/kWh and 7.15km/kWh). The opposite is the case with Tesla Model X and S (6.18 and 6.10km/kWh). By far the largest ranges are recorded for Toyota Mirai and Mercedes EQS. Only BMWi4 and Mercedes EQE can develop speeds higher than 200km/h. The charging costs per one re-charge are the most unfavorable in case of Tesla Model S and BMWi4 (€10.8 and €7.2) while they are the lowest for Tesla Model X and Toyota Mirai (€3.2 and €4.68, respectively). Just for illustration, with the same amount of money for recharging, Tesla

Model S, Volkswagen ID. Buzz, and BMW i4 can pass significantly lower distances than Tesla Model X and Toyota Mirai. Tesla Model S and Tesla Model X are at the top in terms of battery capacity (after Mercedes EQS), however both cars are at the bottom in terms of both efficiency and range. In both aspects they rank as the fourth and fifth best solutions. However, the differences in charging costs make a significant difference for prospective customers. With the same amount of money Tesla Model X can pass the distance that is three times longer than that passed with Tesla Model S. BMW i4's battery ranks as the third worst solution within this capacity, so despite its best efficiency it shares the fourth place with Tesla Model X in terms of range. Taking into consideration the charging costs, which are the second most unfavorable in this range category, BMW i4 can be seen as the second least favorable option for customers. On the other hand, Toyota Mirai follows Tesla Model X in terms of range per the same amount of money so it can be seen as the most attractive option for the customers, especially if we take into consideration that it is cheaper than Tesla Model X for about €30.000. The efficiency of this model is not documented in the selected source, but it has the best range in this category and second best charging costs.

Comparative analysis of different categories

Based on the mean values obtained for each category we can conduct a brief comparative analysis. The obtained values are presented in Table 6.

Table 6 *Technical properties and economic indicators across different range categories*

Range category [km]	Price [€]	Battery size [kWh]	Efficiency [km/ kWh]	Range [km]	Charging costs per charge [€]
200 – 300	30,412	37.29	6.82	242	3.78
300 – 400	49,384	57.36	6.45	339	5.42
400 – 500	40,416	69.91	6.25	436	6.0
> 500	84,295	90.30	6.71	635	6.14

The results show that the mean prices at least partially correspond to the range. As the ranges increase, so does the price. The only exception are the cars with the range 300 – 400km and 400 – 500km. The latter are cheaper than the previous category. As the ranges increase, so does the mean battery capacity. Even though the cars with higher ranges are notorious for being not efficient enough as cars with lower ranges, this analysis shows that the mean values differ slightly. The selection of the top representatives confirms the same. In the first category (200 – 300km), the best efficiencies are reported for Volkswagen e-UP! and SEAT Mii Electric (8.42 km/kWh). With 8.22km/kWh and 7.72km/kWh, Hyundai IONIQ Electric (300 – 400km) and Tesla Model 3 (400 – 500km) follow this trend. The best efficiency within the range >500km is reported for BMW i4 (7.29km/kWh). The main reasons for the discrepancy found with the highest-range models can be attributed to the fact that efficiencies are not documented for four models. Their values could change the image significantly.

These results prove that car industry has been putting serious efforts to create all-electric cars with higher ranges by simultaneously trying to increase their efficiency. In other words, even though they have kept larger batteries needed for long-range drives, they found a way to make their cars more efficient. Obviously, long-range cars still cannot compete with short-range models in terms of efficiency, but at least their efficiency is becoming more and more acceptable. Finally, we must highlight that discrepancies between the models within each range category can be tremendous, so we should avoid generalizations.

4. CONCLUSIONS

This paper summarizes the main properties and economic indicators of 63 all-electric cars that are currently commercially available. The prices differ drastically, as with conventional cars. However, with conventional cars most customers predominantly know what to look for in a car, while the properties of electric cars remain a mystery for laymen. In addition, the car properties which are theoretically the most crucial ones (energy-efficiency and eco-friendliness) are not the most relevant for prospective customers.

Economic indicators must be taken into account because the budget narrows down the selection. In addition, charging costs may be the second most relevant factor since customers desire to make lucrative investments. Thus, we must find ways to evaluate model performances by combining these four features. This paper demonstrates that the best performances are found in those models which have a favorable combination of price, battery capacity, model efficiency, range and charging costs. These factors are interrelated and since there is no objective measure to calculate their impact, we must invent new ways of comparing them. Namely, this paper demonstrates that the highest battery capacity is very frequently not a guarantee that models will have neither the highest efficiency nor the highest range. The results also show that prices of cars, with all other properties being practically identical, can differ significantly if a car offers better speed and acceleration, or is produced by a company with long tradition and good reputation. We have also found the examples that further confirm our hypothesis about the relevance of charging costs. Namely, there are a few examples in which different charging costs are the most drastic difference between two models that otherwise have similar specifications. First, if for the same amount of money a car can pass longer distances, it means that it will be re-charged less frequently. This can be extremely appealing for prospective customers.

The paper also demonstrates that prices do increase with increases in range. Batteries also increase significantly, but efficiencies decrease slightly. Charging costs also increase due to battery size. It is interesting to note that in the first category analyzed here, the most favorable interplay of technical properties and economic indicators is found in the cheapest models (Volkswagen e-UP!, Dacia Spring, and SEAR Mii Electric) because these cars have lower ranges, smaller batteries, and higher efficiency. In the second category, the most appealing interactions of the features are found in the models whose prices are the lowest. The only exception is Hyndai IONIQ Electric, whose price fluctuates around the mean value. The added price can be contributed to the smallest battery, and the highest efficiency. However, in the third and fourth category, the best combinations of the most relevant features are detected in pricier, but not necessarily the most expensive, models.

Finally we must conclude that the slight mean differences in efficiency between short-range and long-range cars are extremely encouraging. This proves that the car industry has been investing a lot of effort to reconcile what customers want (i.e. higher ranges) with what we all need (i.e. energy-efficient and eco-friendly transportation). Their attempts give results and strengthen the vision that that future of car industry is electric.

ACKNOWLEDGMENT

Authors acknowledge the Ministry of Education, Science and Technological Development of the Republic of Serbia for the support through Contracts No. 451-03-9/2021-14/200378 and 451-03-9/2021-14/200107.

REFERENCES

[1] Eurostat, European Commission, https://ec.europa.eu/eurostat.

[2] IEA, International Energy Agency, https://www.iea.org/.

[3] Gómez Vilchez, J., Jochem, P., Fichtner, W.: "Interlinking major markets to explore electric car uptake", Energy Policy, 2020, Vol. 144.

[4] Eltoumi, F. M., Becherif, M., Djerdir, A., Ramadan, H.S.: "The key issues of electric vehicle charging via hybrid power sources: Techno-economic viability, analysis, and recommendations", Renew Sustain Energy Rev, 2020, Vol. 110534.

[5] Thurner, T., Fursov, K., Nefedova, A.: "Early adopters of new transportation technologies: Attitudes of Russia's population towards car sharing, the electric car and autonomous driving", Transp. Res. Part A: Policy and Practice, 2022, Vol. 155, pp. 403-417.

[6] Schmalfuß, F., Mühl, K., Krems, F.J.: "Direct experience with battery electric vehicles (BEVs) matters when evaluating vehicle attributes, attitude and purchase intention", Transp. Res. Part F: Traffic Psychol. Behav., 2017, Vol. 46, pp. 47-69.

[7] Skippon, S.M., Kinnear, N., Lloyd, L., Stannard, J.: "How experience of use influences mass-market drivers' willingness to consider a battery electric vehicle: A randomised controlled trial", Transp. Res. Part A: Policy Practice, 2016, Vol. 92, pp. 26-42.

[8] Hoen, A., Koetse, J.M.: "A choice experiment on alternative fuel vehicle preferences of private car owners in the Netherlands", Transp. Res. Part A: Policy Practice, 2014, Vol. 61, pp. 199-215.

[9] Lieven, T.: "Policy measures to promote electric mobility – a global perspective", Transp. Res. Part A Policy Pract, 2015, Vol.82, pp. 78-93.

[10] Contestabile, M., Alajaji, M., Almubarak, B.: "Will current electric vehicle policy lead to cost-effective electrification of passenger car transport?", Energy Policy, 2017, Vol. 110, pp. 20-30.

[11] Jain, D.: "Viability assessment of electric cars for personal use in India", IATSS Research, 2021.

[12] Rotaris, L., Giansoldati, M., Scorrano, M.: "The slow uptake of electric cars in Italy and Slovenia. Evidence from a stated-preference survey and the role of knowledge and environmental awareness", Transp. Res. Part A Policy Practice, 2021, Vol. 144, pp. 1-18.

[13] Rezvani, Z., Jansson, J., J.: "Advances in consumer electric vehicle adoption research: A review and research agenda", Transport. Res. part D: Transport Environment, 2015, Vol. 34, pp. 122-136.

[14] Liao, F., Molin, E., van Wee, B.: "Consumer preferences for electric vehicles: a literature review", Transport Reviews, 2017, Vol. 37, pp. 252-275.

[15] Kumar, R.R., Alok, K.: "Adoption of electric vehicle: A literature review and prospects for sustainability", J. Cleaner Prod, 2020, Vol. 253, No. 119911.

[16] Mutarraf, U.M., Guan, Y.: "Electric cars, ships, and their charging infrastructure – A comprehensive review", Sustainable Energy Technologies and Assessments, 2022, Vol. 52, No. 119911.

[17] https://ourworldindata.org/grapher/electricity-prod-source-stacked?country=~SRB.

[18] IEA, International Energy Agency, URL: https://www.iea.org/data-and-statistics/charts/global-sales-and-sales-market-share-of-electric-cars-2010-2021, [cited 01.03.2022].

[19] Mitić, S., Blagojević, I., Stamenković, D.: "Vehicle legislation – Serbia vs. Europe", Mobility & Vehicle mechanics (MVM), 2021, Vol. 47, No. 4.

[20] Sommer, S., Vance, C.: "Do more chargers mean more electric cars?", Tech. rep., Ruhr Economic Papers, 2021.

[21] Regulatory environment and incentives for using electric vehicles and developing a charging infrastructure, URL: https://www.bmwi.de/Redaktion/EN/Artikel/Industry/regulatory-environment-and-incentives-for-using-electric-vehicles.html, [cited 18.04.2022].

[22] Inspiration|Electric and Hybrid Vehicles|Electrifying URL: https://www.electrifying.com/inspiration, [cited 03.03.2022].

[23] Elektroprivreda Srbije, zvanična internet stranica, http://www.eps.rs/cir, [cited 12.03.2022].

[24] AMS Automotosavez - https://www.amss.org.rs/.

MOBILITY & VEHICLE MECHANICS

DOI: 10.24874/mvm.2022.48.01.03
UDC:629.3.024.61

THE BUCKLING ANALYSIS OF A ELASTICALLY CLAMPED RECTANGULAR PLATE

Ivan Miletić [1], Marko Miletić [2], Saša Milojević [3], Robert Ulewicz [4], Ružica Nikolić [5]*

Received in October 2020 *Accepted in January 2022*

RESEARCH ARTICLE

ABSTRACT: The paper analyses the stability of a rectangular plate which is elastically buckled along longitudinal edges and pressed by equally distributed forces. A general case is analysed – different stiffness elastic clamping and then special simpler cases are considered. Energy method is used in order to determine critical stress. Deflection function is introduced in a convenient way so that it reflects the actual state of the plate deformation in the best manner. In this way, critical stress is determined in analytic form suitable for analysis. With help of the equation it is easy to conclude how certain parameters influence the value of critical stress. The paper indicates how the obtained solution could be utilized for determining local buckling critical stress in considerably more complex systems – pressed thin-walled beams of an arbitrary length.

KEY WORDS: *buckling, rectangular plate, thin-walled beams*

[1]*Ivan MIletić, PhD, Associate professor, University of Kragujevac, Faculty of Engineering, Sestre Janjić 6, 34000 Kragujevac, Serbia, imiletic@kg.ac.rs, https://orcid.org/0000-0002-1935-5771 (*Corresponding author)*
[2]*Marko Miletić, PhD, University of Kragujevac, Faculty of Engineering, Sestre Janjić 6, 34000 Kragujevac, Serbia, marko.m.miletic@hotmail.com*
[3]*Saša Milojević, Expert advisor, University of Kragujevac, Faculty of Engineering, Sestre Janjić 6, 34000 Kragujevac, Serbia, sasa.milojevic@kg.ac.rs, https://orcid.org/0000-0003-0569-047X*
[4]*Robert Ulewicz, PhD, Associate professor, Częstochowa University of Technology, Department of Production Engineering and Safety, 42201 Częstochowa, Poland, robert.ulewicz@wz.pcz.pl, https://orcid.org/0000-0002-5694-4284*
[5]*Ružica Nikolić, PhD, Full professor, University of Žilina, Research Center, 010 26 Žilina, Slovakia, ruzica.nikolic@rc.uniza.sk, https://orcid.org/0000-0003-3042-8916*

ANALIZA IZVIJANJA ELASTIČNO STEGNUTE PRAVOUGAONE PLOČE

REZIME: U radu je analizirana stabilnost pravougaone ploče koja je elastično izvijena duž uzdužnih ivica i pritisnuta podjednako raspoređenim silama. Analizira se opšti slučaj – različite krutosti tokom elastičnog uklje序tenja, a zatim se razmatraju posebni jednostavniji slučajevi. Energetski metod se koristi za određivanje kritičnog napona. Funkcija otklona je uvedena na odgovarajući način tako da na najbolji način odražava stvarno stanje deformacije ploče. Na ovaj način se kritični napon određuje u analitičkom obliku pogodnom za analizu. Uz pomoć jednačine lako je zaključiti kako pojedini parametri utiču na vrednost kritičnog napona. U radu je prikazano kako bi se dobijeno rešenje moglo koristiti za određivanje kritičnog napona lokalnog izvijanja u znatno složenijim sistemima – presovanim tankozidnim gredama proizvoljne dužine.

KLJUČNE REČI: *izvijanje, pravougaona ploča, tankozidne grede*

THE BUCKLING ANALYSIS OF A ELASTICALLY CLAMPED RECTANGULAR PLATE

Ivan Miletić, Marko Miletić, Saša Milojević, Robert Ulewicz, Ružica Nikolić

INTRODUCTION

In researching so called local buckling of thin-wall prismatic beams under a uniform compression load over the cross-section area, a problem occurs with determining critical stress, with the entire element as a whole as well as in individual rectangular plates which make up the element. The plates which make up the element are connected along the mating lines, therefore when looking at the stability of specific plates the influence of adjacent plates cannot be overlooked. Adjacent plates when loaded axially in this configuration act like elastic clamping, they load the given plate with bending moments evenly distributed along the mating lines. These moments are [1, 2] proportional to the plate bend on those edges, and the coefficient of proportionality C – stiffness of elastic clamping – depend on the adjacent plates to which the plate is connected. These cases occur when observing stability of any thin-walled beam with a rectangular cross-section contour, as well as when considering rib stability of thin-walled beams with a U and Z cross-section. Buckling calculations of beam elements is an indispensable part of calculating all axially loaded structures [3-6].

1. ANALYSIS OF A PLATE ELASTICALLY CLAMPED ALONG THE EDGES

The problem considered in this research is buckling of beams which is based on the analysis of the buckling of a rectangular elastically clamped plate whose length is equal to the length of the beam, and the width b is equal to the length of the contour line of the profile (Figure 1) [7]. The plate is elastically clamped along the longitudinal edges.

The stiffness of elastically clamped longitudinal edges are different on either side (there is no symmetry of the system, it is considered to be a general case) and continuous along the edge of the plate. Along the other two loaded edges the plate is freely placed.

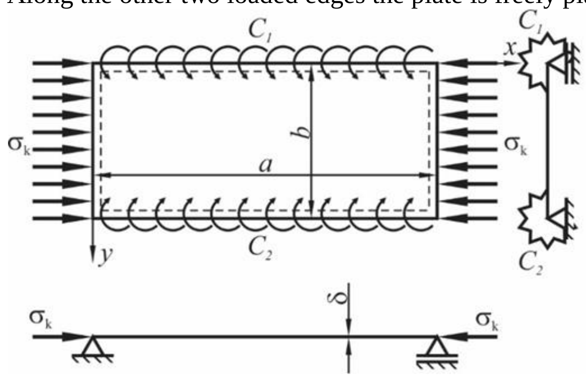

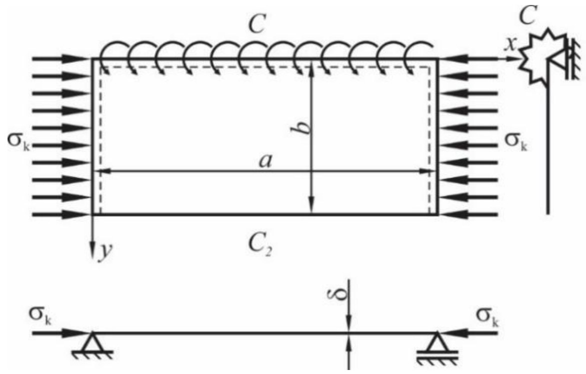

Figure 1 Plate supports

Buckling of the plate in the longitudinal direction, due to the way it is supported, can be presented as a sinusoid using the following expression:

$$f(x) = \sin\frac{m\pi x}{a} \tag{1}$$

Plate buckling in the transverse direction is determined by the use of superposition of the free support, when the buckling can represent a sinusoidal function, and the buckling of two "elastic" moments:

$$f(y) = \sin\frac{\pi y}{b} - N_1\left(2b^2y - by^2 + y^3\right) - N_2\left(b^2y - y^3\right) \tag{2}$$

Deflection of the buckled plate can be represented using the following expression:

$$w = Af(x)f(y) = A\sin\frac{m\pi x}{a}\left[\sin\frac{\pi y}{b} - N_1\left(2b^2y - by^2 + y^3\right) - N_2\left(b^2y - y^3\right)\right] \tag{3}$$

where: *A* – constant (buckling amplitude); *x, y* – longitudinal and transversal coordinate; *m* – number of longitudinal half-waves of the deformed plate ***(m*** $\in \mathbb{N}$***); N_1*** and $\mathbf{N_2}$ – constants which are determined from limit conditions.

Bending moments of the plate on the edges must be equal to the moments of the elastic clamping:

$$\begin{aligned} -D\left(\frac{\partial^2 w}{\partial y^2} + \mu\frac{\partial^2 w}{\partial x^2}\right)_{y=0} &= C_1\left(\frac{\partial^3 w}{\partial x^2 \partial y}\right)_{y=0}, \\ -D\left(\frac{\partial^2 w}{\partial y^2} + \mu\frac{\partial^2 w}{\partial x^2}\right)_{y=b} &= -C_2\left(\frac{\partial^3 w}{\partial x^2 \partial y}\right)_{y=b}. \end{aligned} \tag{4}$$

where $D = \frac{E\delta^3}{12\left(1-\mu^2\right)}$ – plate bending stiffness (E – Young modulus, μ - Poisson coefficient).

From these conditions (4) constants N_1 and N_2 are derived to have the following values:

$$\begin{aligned} -D\left(\frac{\partial^2 w}{\partial y^2} + \mu\frac{\partial^2 w}{\partial x^2}\right)_{y=0} &= C_1\left(\frac{\partial^3 w}{\partial x^2 \partial y}\right)_{y=0}, \\ -D\left(\frac{\partial^2 w}{\partial y^2} + \mu\frac{\partial^2 w}{\partial x^2}\right)_{y=b} &= -C_2\left(\frac{\partial^3 w}{\partial x^2 \partial y}\right)_{y=b}. \end{aligned} \tag{5}$$

that is:

$$N_1 = \frac{m^2\pi^3\overline{C_1}\left(6+m^2\pi^2\overline{C_2}\right)}{3b^3\left(12+4m^2\pi^2\overline{C_1}+4m^2\pi^2\overline{C_2}+m^4\pi^4\overline{C_1}\,\overline{C_2}\right)},$$
$$N_2 = \frac{m^2\pi^3\overline{C_2}\left(6+m^2\pi^2\overline{C_1}\right)}{3b^3\left(12+4m^2\pi^2\overline{C_1}+4m^2\pi^2\overline{C_2}+m^4\pi^4\overline{C_1}\,\overline{C_2}\right)}. \tag{6}$$

where $\overline{C_1} = \dfrac{bC_1}{a^2D}$ and $\overline{C_2} = \dfrac{bC_2}{a^2D}$ - is reduction (non-dimensional) of the elastic clamping stiffness. With joint supports $C_1 = C_2 = 0$, $\overline{C_1} = \overline{C_2} = 0$, and $N_1 = N_2 = 0$, and with clamping it is $C_1 = C_2 = \infty$, $\overline{C_1} = \overline{C_2} = \infty$, $N_1 = \dfrac{\pi}{3b^3}$ and $N_2 = \dfrac{\pi}{3b^3}$. In the general case $0 \le N_1 \le \dfrac{\pi}{3b^3}$ and $0 \le N_2 \le \dfrac{\pi}{3b^3}$.

Potential energy of the system van be determined as a sum of potential energies of the plate and the potential energy of the elastic clamps:

$$E_p = \frac{D}{2}\int_0^a\int_0^b\left\{\left(\frac{\partial^2 w}{\partial x^2}+\frac{\partial^2 w}{\partial y^2}\right)^2 - 2(1-\mu)\left[\frac{\partial^2 w}{\partial x^2}\frac{\partial^2 w}{\partial y^2}-\left(\frac{\partial^2 w}{\partial x\partial y}\right)^2\right]\right\}dxdy + \int_0^a\left(\frac{M_1^2}{2C_1}\right)dx + \int_0^a\left(\frac{M_2^2}{2C_2}\right)dx \tag{7}$$

In this case buckling was considered using function (3) and that moments are $M_1 = C_1\left(\dfrac{\partial^2 w}{\partial x\partial y}\right)_{y=0}$ and $M_2 = -C_2\left(\dfrac{\partial^2 w}{\partial x\partial y}\right)_{y=a}$.

Work of external forces is:

$$A_d = \frac{1}{2}\sigma_k\delta\int_0^a\int_0^b\left(\frac{\partial w}{\partial x}\right)^2 dxdy \tag{8}$$

By equating the potential energies in the system (7) and the work of external forces (8) critical load can be given as:

$$\sigma_k = \frac{D\pi^2}{b^2\delta}k \tag{9}$$

where k is the buckling coefficient:

$$k = m^2\left(\frac{b}{a}\right)^2 + \frac{1}{m^2}\left(\frac{a}{b}\right)^2 Q + R \tag{10}$$

and P and Q are dimensionless constants:

$$P = 105\frac{\left[12+4m^2\pi^2\left(\overline{C_1}+\overline{C_2}\right)+m^4\pi^4\overline{C_1}\,\overline{C_2}\right]\left[12+\left(4m^2\pi^2-24m^2\right)\left(\overline{C_1}+\overline{C_2}\right)+\left(m^4\pi^4-8m^4\pi^2\right)\overline{C_1}\,\overline{C_2}\right]}{\begin{array}{c}15120+10080m^2\left(\pi^2-6\right)\left(\overline{C_1}+\overline{C_2}\right)+16m^4\pi^2\left(105\pi^2+4\pi^4-1260\right)\left(\overline{C_1}^2+\overline{C_2}^2\right)+\\ +4m^4\pi^2\left(1470\pi^2+31\pi^4-15120\right)\overline{C_1}\,\overline{C_2}+\\ +42m^6\pi^4\left(20\pi^2+\pi^4-280\right)\left(\overline{C_1}^2\overline{C_2}+\overline{C_1}\,\overline{C_2}^2\right)+7m^8\pi^6\left(15\pi^2+\pi^4-240\right)\overline{C_1}^2\overline{C_2}^2\end{array}}, \tag{11}$$

$$Q = 14\frac{\begin{gathered}2160 + 1440m^2\left(\pi^2-6\right)\left(\overline{C}_1+\overline{C}_2\right) + 48m^4\pi^2\left(7\pi^2-60\right)\left(\overline{C}_1^{\,2}+\overline{C}_2^{\,2}\right) + 144m^4\pi^2\left(7\pi^2-60\right)\overline{C}_1\overline{C}_2 + \\ +60m^6\pi^4\left(3\pi^2-28\right)\left(\overline{C}_1^{\,2}\overline{C}_2+\overline{C}_1\overline{C}_2^{\,2}\right) + \\ +5m^8\pi^6\left(5\pi^2-48\right)\left(\overline{C}_1^{\,2}\overline{C}_2^{\,2}\right)\end{gathered}}{\begin{gathered}15120 + 10080m^2\left(\pi^2-6\right)\left(\overline{C}_1+\overline{C}_2\right) + 16m^4\pi^2\left(105\pi^2+4\pi^4-1260\right)\left(\overline{C}_1^{\,2}+\overline{C}_2^{\,2}\right) + \\ +4m^4\pi^2\left(1470\pi^2+31\pi^4-15120\right)\overline{C}_1\overline{C}_2 + \\ +42m^6\pi^4\left(20\pi^2+\pi^4-280\right)\left(\overline{C}_1^{\,2}\overline{C}_2+\overline{C}_1\overline{C}_2^{\,2}\right) + 7m^8\pi^6\left(15\pi^2+\pi^4-240\right)\overline{C}_1^{\,2}\overline{C}_2^{\,2}\end{gathered}}. \quad (12)$$

Buckling coefficients for some extreme cases of supports (joints along all for edges, clamping along one plate edge and clamping on other edges, as well as two sided clamping) are the same as values given in [6]. For the case of elastic supports the coefficient of buckling is determined by the expressions given in Figure 2.

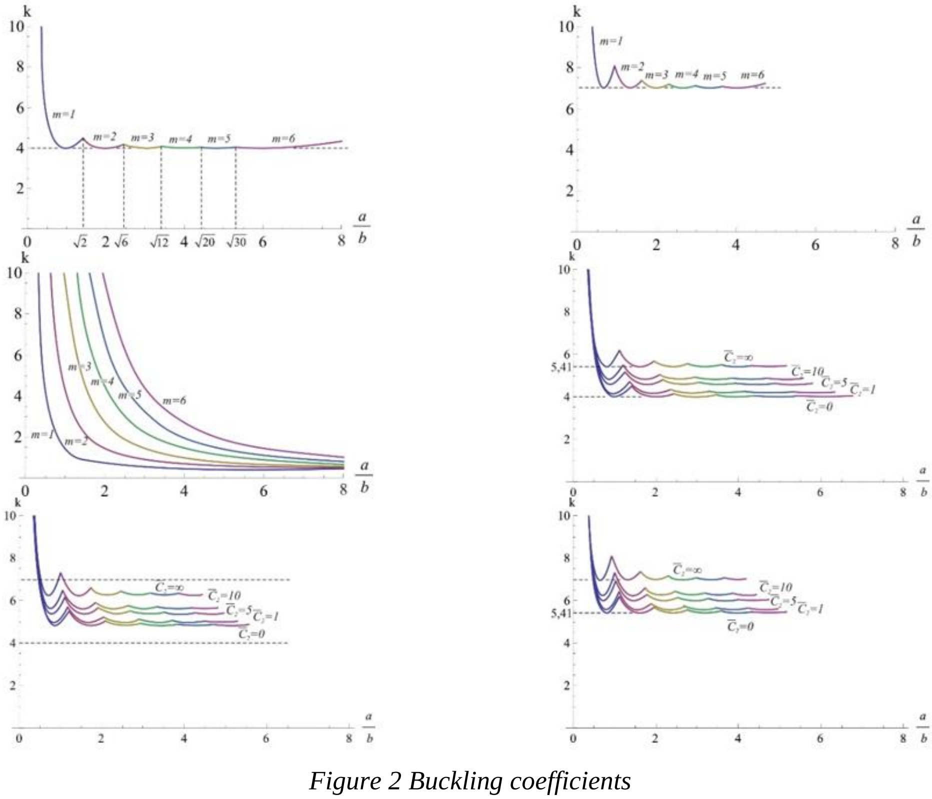

Figure 2 Buckling coefficients

2. TORSION STIFFNESS

In order to calculate the local buckling stress in general cases of elastically clamped plates and to use them in analysis of the plate's stability the torsion stiffness must be determined for buckling of prismatic shells. It is important to note that prismatic shell loses stability as a whole the instant when the weakest plate loses stability, that is to say that if the shell consists of ribs and an outer shell, the shell loses its stability when any one of the ribs or the outer shell loose stability. Figure 3 shows two general forms of plate with elastic clamping, as well as the shape used for each case of prismatic shell [6, 7]. One form is the plate freely supported along the edges which are under load and elastically supported along the longitudinal edges, and the other is a plate freely supported along the edges which are under load, elastically supported along one and free along the other longitudinal edge. Equations for determining critical buckling stress for these two support cases are determined in the previous heading of this paper [8, 9]. When analyzing plates which are integral parts of the shell, regardless of the load-case it is necessary to introduce a correctional factor [9, 10]:

$$r = 1 - \frac{\sigma_{restriktied\ plate}}{\sigma_{restraining\ plate}} \tag{13}$$

In the case of buckling equation (12) is given as:

$$r = 1 - \frac{\sigma_k^{restricted\ plate}}{\sigma_k^{restraining\ plate}} \quad x = a^2 + b_1 + \sum \varepsilon_i \alpha \tag{14}$$

It is important to note that when calculating correctional factors for critical stress of limited and limiting plates the critical stress of the plate with the free support, that is the freely supported plate and plate whose one edge is free and the other is freely supported.

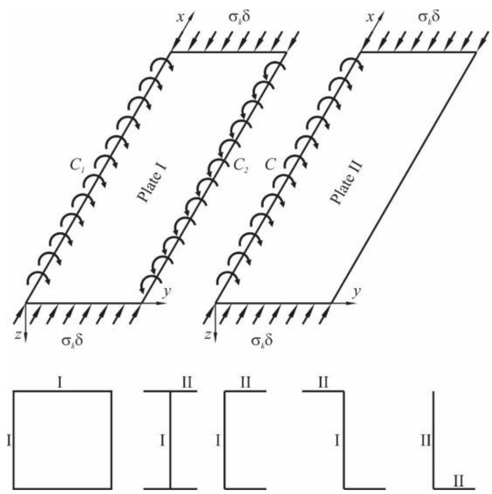

Figure 3 Elastically clamped plates

Torsional stiffness for rectangular profiles is:

$$C = \frac{2m\pi D\left[\cosh\left(\frac{b_r m\pi}{a}\right)-1\right]}{a\sinh\left(\frac{b_r m\pi}{a}\right)-b_r m\pi}\left(1-\frac{b_r^4}{b_p^4}\frac{\left(a^2+b_p^2\right)^2}{\left(a^2+b_r^2\right)^2}\right) \quad x = a^2 + b_1 + \sum \varepsilon_i \alpha \tag{15}$$

While when using I profiles:

$$C=\frac{2m\pi D\left[a\sinh\left(\frac{2b_p m\pi}{a}\right)-2b_p m\pi\right]}{7a^2-2b_p^2m^2\pi^2+a^2\cosh\left(\frac{2b_p m\pi}{a}\right)}\left\{1-\frac{b_p^2\left(a^2+b_r^2m^2\right)^2\pi^2}{b_r^4m^2\left[b_p^2m^2\pi^2+6a^2\left(1-\mu\right)\right]}\right\} \tag{16}$$

When using Z and U profiles

$$C=\frac{2m\pi D\left[a\sinh\left(\frac{2b_p m\pi}{a}\right)-2b_p m\pi\right]}{7a^2-2b_p^2m^2\pi^2+a^2\cosh\left(\frac{2b_p m\pi}{a}\right)}\left\{1-\frac{b_p^2\left(a^2+b_r^2m^2\right)^2\pi^2}{b_r^4m^2\left[b_p^2m^2\pi^2+6a^2\left(1-\mu\right)\right]}\right\} \tag{17}$$

3. NUMERICAL CALCULATION

For validation of the results calculated in the previous heading available data from literature was used (analytical and experimental data) and numerical analysis using the finite element method (FEM). Pre-processing and post-processing in the FEM analysis was done in FEMAP software, and processing was done in NXNastran which is integrated in FEMAP. For solving this problem the default input settings were used.

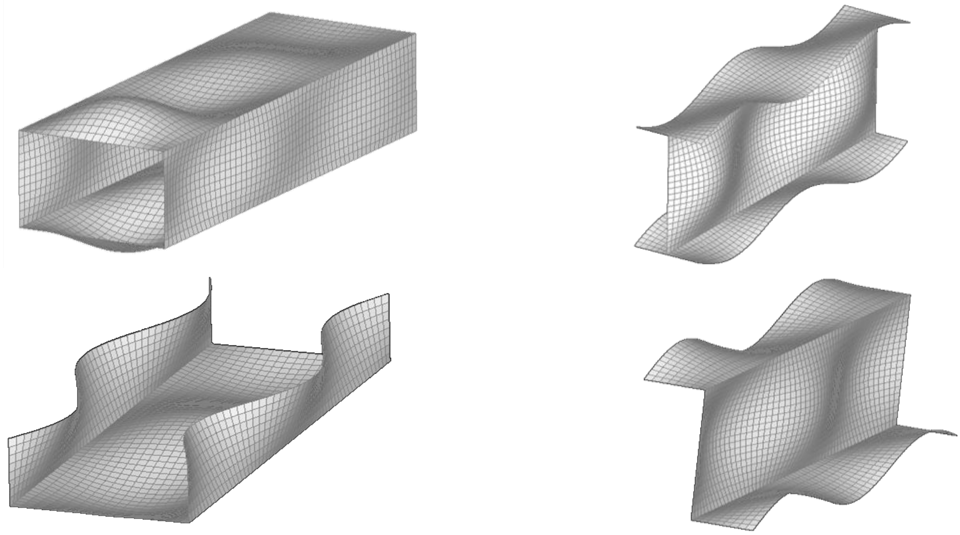

Figure 4 FEA results

The greatest variation recorded is 8.55%, therefore the analytical calculation equations can be considered acceptable for stability calculation. Verification of data with literature also confirms coincidence with the results from the literature are in the range of 5.5% [6, 7] and [11-13].

4. CONCLUSIONS

The use of equations for determining torsional rigidity give equations for determining critical buckling stress of various thin-walled profiles which represent prismatic shells. By analysing the equations for determining critical stress of rectangular profiles it can be

concluded that rectangular profiles will always buckle along the wider side. In the case of square profiles there is no influence of elastic supports however the plates which make up the profile act as freely supported plates. By decreasing the width of the narrow sides the influence on the stability of the wider sides increases, and with it the influence on the shell stability. In the limiting cases when the width of the narrower sides is converging to zero the elastic supports act as regular supports. By analysing the equations for determining critical loads for U and Z profiles the following conclusions can be made. Thin walled beams which use U and Z profiles can be found in two cases depending on the proportions of the outer shell and ribs. The first case is when the outer shell buckles first and when the rib profile represents the limiting element. This is the case when the width ratio of outer shell to rib is greater than 0.36847. As the width ratio increases over this value the influence of the rib is lessened. In the case that the width ratio is equal to this number there is no mutual influence of the rib and outer shell and they function as if they are freely supported plates. The other case is when the rib buckles first and the limiting element is the outer shell. This is the case when the width ratio of outer shell to rib is less than 0.36847. By decreasing this ratio the system stiffness increases up to the point when the ratio reaches 0.2. Further decreasing of the ratio leads to a decrease in rib stiffness and when the rib width converges to zero the influence is completely lost. These results are used in data taken from literature.
Analysing I profiles the same conclusions can be made as with the U and Z profiles, except in this case half the belt width is used. When analysing L profiles the first to buckle is always the wider rib. When the ribs are equal widths there is no influence of the elastic support. Torsional stiffness is negligible (the maximal value of reduced torsional stiffness is 0.7795). Due to this it is understandable why in literature only uneven L profiles can be found.

ACKNOWLEDGMENT

This paper presents results obtained within realization of the projects TR-33015 funded by Ministry of Education, Science and Technological Development of the Republic of Serbia and the project of Operational Program Research and Innovation: “Research and development activities of the University of Žilina in Industry of the 21st century in the field of materials and nanotechnologies”, No. 313011T426, co-funded by the European Regional Development Fund.

REFERENCES

[1] Timoshenko, S.P.: “Theory of Elastic Stability”, McGraw-Hill Book Company, inc., New York and London, 1936.

[2] Pflüger, A.: “Stabilitätsproblme der Elostostatik”, Springer-Verlag, Berlin-Göttingen-HeidelbergNew York, 1964.

[3] Euler, L.: “Methodus inveniendi lineas curvas maximi minimive proprietate gaudentes, sive solutio problematis isoperimetrici lattissimo sensu accepti”, Lausanne, 1774.

[4] Teter, A.: “Static and dynamic interactive buckling of isotropic thin-walled closed columns with variable thickness”, Thin-Walled Struct, 2007, pp. 936–940, doi: 10.1016/j.tws.2007.08.021.

[5] Wolfram, S.: “The Mathematica”, Book – 5 th edition, Wolfram Media 2003.

[6] Miletić, I.: “Stabilnost aksijalno pritisnutih prizytičnih ljuski”, Magistarski rad, Mašinski fakultet u Kragujevcu, 2009.

[7] Miletić, I., Miletić, M.: “The buckling analysis of a rectangular plate elastically clamped along the longitudinal edges”, Applied Engineering Letters, 2016, Vol. 1, No. 1, pp. 24-28.

[8] Bogdanović, G., Milosavljević, D., Radaković, A., Čukanović, D., Geroski, V.: “Acoustical tensor and elastic wave propagation in anisotropic materials used in automotive industry “, Mobility & Vehicle Mechanics, 2017, Vol. 43, No. 3, pp. 65-71.

[9] Teter, A.: “Coupled dynamic buckling of thinwalled composite columns with open crosssections”, Thin-Walled Structures, 2011, pp. 589–595.

[10] Fenner, P.E., Watson, A.: “Finite element buckling analysis of stiffened plates with filleted junctions”, Thin-Walled Structures, 2012, pp 171–180.

[11] Petrović, N., Kostić, N., Marjanović, N., Živković, J., Cofaru, I.I.: “Effects of structural optimization on practical roof truss construction”, Applied Engineering Letters: Journal of Engineering and Applied Sciences, 2020, Vol. 5, No. 2, pp. 39-45, doi: 10.18485/aeletters.2020.5.2.1.

[12] Petrovic, N., Marjanovic, N., Kostic, N., Blagojevic, M., Matejic, M., Troha, S.: “Effects of introducing dynamic constraints for buckling to truss sizing optimization problems”, FME Transaction, 2018, Vol. 46, pp. 117-123, doi: 10.5937/fmet1801117P.

[13] Petrovic, N., Kostic, N., Marjanovic, N.: “Discrete variable truss structural optimization using buckling dynamic constraints”, Machine Design, 2018, Vol. 10, pp. 51-56. Doi: 10.24867/MD.10.2018.2.51-56.

MOBILITY & VEHICLE MECHANICS

DOI: 10.24874/mvm.2022.48.01.04
UDC:629.3.015.5

EFFECT OF VIBRATION ON SEMICIRCULAR CANAL DURING WHOLE BODY VIBRATION

Slavica Mačužić Saveljić [1], Igor Saveljić [2], Nenad Filipović [3]*

Received in April 2022 *Accepted in May 2022*

RESEARCH ARTICLE

ABSTRACT: Chronic exposure to whole body vibration can affect the lumbar spine, the gastrointestinal system, the peripheral veins and the vestibular system. The semicircular canals (SSC), as a part of vestibular system, are responsible for sensing angular head motion in three-dimensional space and for providing neural inputs to the central nervous system. In this paper, the influence of random vibration on the body of the subject at an excitation of 1.0 m/s^2 and 1.5 m/s^2 was investigated. The 3D geometry of the SSC canal was obtained using DICOM CT images. Simulation of endolymph flow is carried out. Numerical analysis provides the pressure generated on SSC. Response of cupula is obtained for various rotational velocities of head. Variation of pressure generated on cupula and response of cupula is studied and reported.

KEY WORDS: *numerical analysis, random vibration, semicircular canals, whole body vibration*

[1] *Slavica Mačužić Saveljić, Assistant, University of Kragujevac, Faculty of Engineering, Sestre Janjić 6, 34000 Kragujevac, Serbia, s.macuzic@kg.ac.rs, https://orcid.org/0000-0003-2635-2496 (*Corresponding author)*

[2] *Igor Saveljić, PhD, University of Kragujevac, Institute for Information Technologies, Jovana Cvijića bb, 34000 Kragujevac, Serbia, isaveljic@kg.ac.rs, https://orcid.org/0000-0002-0707-5174*

[3] *Nenad Filipovic, PhD Professor, University of Kragujevac, Faculty of Engineering, Sestre Janjić 6, 34000 Kragujevac, Serbia, fica@kg.ac.rs, https://orcid.org/0000-0001-9964-5615*

UTICAJ VIBRACIJA CELOG TELA NA POLUKRUŽNI KANAL UHA

REZIME: Hronična izloženost vibracijama celog tela može uticati na lumbalni deo kičme, gastrointestinalni sistem, periferne vene i vestibularni sistem. Polukružni kanali (eng. semicircular canals - SSC), kao deo vestibularnog sistema, odgovorni su za detekciju ugaonog kretanja glave u trodimenzionalnom prostoru i za obezbeđivanje neuronskih ulaza u centralni nervni sistem. U ovom radu je ispitivan uticaj nasumičnih vibracija na telo ispitanika pri pobudama od 1.0 m/s^2 i 1.5 m/s^2. 3D geometrija SSC kanala dobijena je korišćenjem DICOM CT slika. Sprovedena je simulacija endolimfnog toka. Numerička analiza pokazuje pritisak koji se stvara u SSC kanalima. Odziv kupule se dobija za različite brzine rotacije glave. Proučavaju se i prikazuju promene pritiska generisanog na kupuli, kao i odziv kupule.

KLJUČNE REČI: *numerička analiza, slučajna vibraija, polukružni kanali, vibracije celog tela*

EFFECT OF VIBRATION ON SEMICIRCULAR CANAL DURING WHOLE BODY VIBRATION

Slavica Mačužić Saveljić, Igor Saveljić, Nenad Filipović

INTRODUCTION

The oscillatory comfort of a vehicle is a complex problem that is influenced by several factors, of which the road characteristics, the mechanical characteristics of the vehicle as well as the speed of the vehicle should be mentioned. In the thirties of the last century, with the rapid development of industrial machines and motor vehicles, the negative effects of the effects of vibrations on the human body were noticed. Much research in recent decades has been devoted to investigating the effects of vibrations and the effects they cause [1], [2], [3]. The reaction of the human body to the action of vertical vibrations can be divided into five different effects, which include: perception of low vibration, nausea while driving, reduced comfort, impaired health and disruption of activity. These effects depend on the manner and degree of vibration transmission through the human body (biomechanical response of the human body). In order to reduce the negative impact of vibrations on humans, the European Union adopted the Vibration Directive (2002/44 / EC) in 2002, which defines the permissible levels of exposure to whole human body vibrations in working conditions and appropriate safety measures to protect health. When describing vibrations, it is important to fully describe what vibration characteristics are involved. To expose the body to vertical vibrations, these are: frequency content, amplitude, direction and length of vibration exposure. A vibration wave may consist of a single frequency wave or it may be as complex as a broadband wave consisting of multiple frequencies. The frequency of vibration waves describes how fast the vibrations move [4], [5]. Exposure to vibrations affects a person in different ways, starting from ordinary disturbances, to reduced work performance and damage to health. A guideline in defining human tolerance to whole-body vibration as an international standard ISO 2631-1 (1997) [6] was adopted today. ISO 2631-5 (2004) [7] is used to assess exposure to high levels of vibration and shock. ISO 2631-4 (2001) [8] is used to define different methods for measuring periodic, random and transient vibrations. The vibrations that are absorbed lead to muscle contractions that can cause muscle fatigue, especially at resonant frequencies. Vertical vibrations in the range of 5–10 Hz cause resonance in the thoracic abdominal system, from 4 - 8 Hz in the spinal part, from 20 - 30 Hz in the area of the head and neck and from 60 - 90 Hz in the area of the eyeballs.

The vestibular system is the sensory apparatus of the inner ear that helps the body maintain its postural equilibrium. The information furnished by the vestibular system is also essential for coordinating the position of the head and the movement of the eyes. There are two sets of end organs in the inner ear, or labyrinth: the semicircular canals, which respond to rotational movements (angular acceleration); and the utricle and saccule within the vestibule, which respond to changes in the position of the head with respect to gravity (Figure 1). The information these organs deliver is proprioceptive in character, dealing with events within the body itself, rather than exteroceptive, dealing with events outside the body, as in the case of the responses of the cochlea to sound. Functionally these organs are closely related to the cerebellum and to the reflex centres of the spinal cord and brainstem that govern the movements of the eyes, neck, and limbs. Because the three semicircular canals - superior, posterior, and horizontal - are positioned at right angles to one another, they are able to detect movements in three-dimensional space. When the head begins to rotate in any direction, the inertia of the endolymph causes it to lag behind, exerting pressure that deflects the cupula in the opposite direction.

Whole body vibrations can weaken the senses and lead to balance disorders, movement disorders or visual disturbances. Periodic vibrations of low frequency of 10-20 Hz show a detrimental effect on the vestibular apparatus [9].

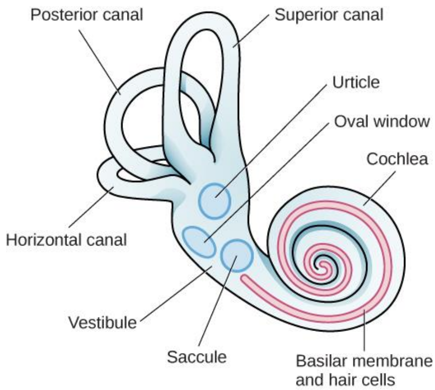

Figure 1 The major sensory organs of the vestibular system - the utricle, saccule, and the three semicircular canals (posterior, superior/anterior, and horizontal) [9]

1. MATERIALS AND METHODS

A healthy human right membranous labyrinth based on the morphologically descriptive model were reconstructed using the CT scans. The high resolution CT data were read into Mimics 17.0 (Materialise Inc., Leuven, Belgium) visualization software, where the images were segmented by thresholding to obtain 3D model (Figure 2).

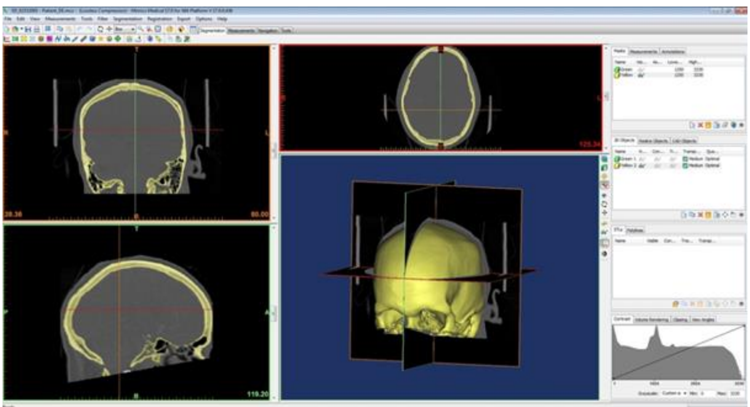

Figure 2 Automatic segmentation of CT scans

The computational model consists of the utricular cavity, the horizontal canal (HC), the anterior canal (AC), the posterior canal (PC), and their ampullae (Figure 3) [10].

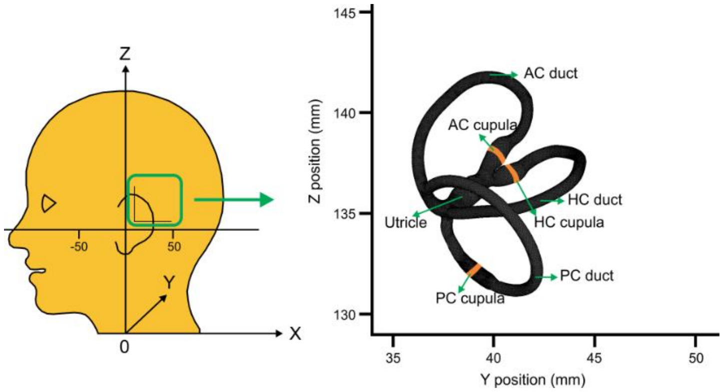

Figure 3 The reconstructed model of a healthy human membranous (the semicircular canals) labyrinth and position in head

The endolymph flow were described by the conservation equations of mass, momentum, and energy. An Arbitrary Lagrangian Eulerian (ALE) approach is adopted, and the endolymph is assumed to be a slightly compressible Newtonian fluid with constant properties. All the governing equations are listed below.
The continuity equation is approximated as [11]:

$$v_{i,i} + \frac{p}{\lambda} = 0 \tag{1}$$

where λ is a selected large number, the penalty parameter. Substituting the pressure p from Eq. 1 into the Navier-Stokes equations it can be obtained

$$p\left(\frac{\partial v_i}{\partial t} + \partial v_{i,k} v_k\right) - \lambda v_{j,ij} - \mu v_{i,kk} - f_i^V = 0 \tag{2}$$

Then the FE equation of balance becomes

$$M\dot{V} + \left(K_{vv} + K_{vv}^{\lambda}\right)V = F_v + F_\lambda \tag{3}$$

where

$$\left[K_{KJ}^{\lambda}\right]_{ik} = \lambda \int_V N_{K,i} N_{J,k} dV, \qquad \left(F_\lambda\right)_{Ki} = \lambda \int_S N_K v_{j,j} n_i dS \tag{4}$$

Fluid-structure interaction for cupula deformation and endolymph flow is implemented. Cupula was modeled as elastic 3D membrane with brick finite element and endolymph domain as 3D 8–node finite elements. The values for the endolymph conductivity, reference density, and viscosity are taken from measured data provided by [12]. The physical and structural properties of the endolymph and cupula are shown in Table 1.

***Table 1** The physical and structural properties of the endolymph and cupula [12]*

Property	Value
Cupula density (kg/m3)	1000
Cupula Young's modulus (Pa)	5
Cupula Poisson ratio	0.45
Endolymph density (kg/m3)	1000
Endolymph dynamic viscosity (Pa·s)	0.000852

In this paper, the HP-2007 electro-hydraulic pulsator were used to induce excitation of different amplitudes and frequencies, which includes a car seat on which the subject were exposed to vibrations. This device has the ability to cause random vibrations in both the vertical and horizontal axes simultaneously. The excitation frequency were in range 0.1-35Hz. Test subject were man of 95 kg and 188 m height. Measuring equipment 01dB-Metravib NetdB PRO-132 was used for signal acquisition. There was an accelerator on the subject's head to determine the head displacements, which are the input values of the acceleration given to the numerical model.

2. RESULTS

Numerical simulation was performed using PAKFS solver. Two cases of acceleration were investigated – 1 m/s^2 and 1.5 m/s^2. The results of velocities and pressures changes in the channels of the vestibular system are shown in the following figures.

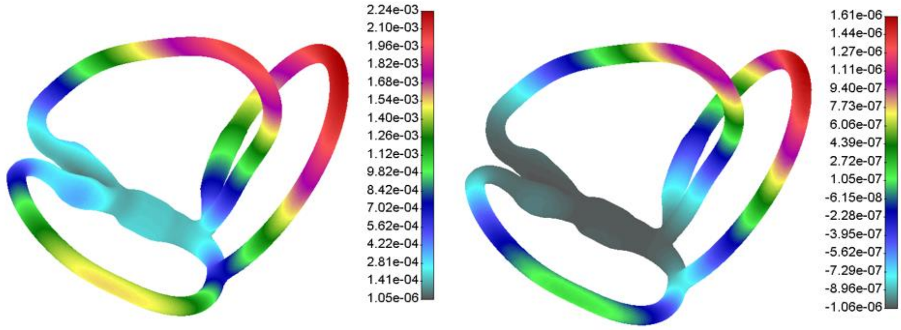

a) b)

Figure 4 The numerical result the velocity (a) and pressure (b) distribution along the human membranous labyrinth during 1 m/s2 acceleration

The figure 4a shows that the highest velocity occurs in the PC duct, 2.24e-03 mm/s, while in the PC cupula measured velocity of 1.12e-03 mm/s. The HC duct has a velocity value of 2.05 m/s^2. The highest pressure of 1.61e-06 Pa, also for the first case of 1 m/s^2, was observed in the PC duct. A slightly lower pressure value was recorded in the HC duct, 9.55e-07 Pa. The second case (Figure 5) showed higher maximum values of both velocity and pressure.

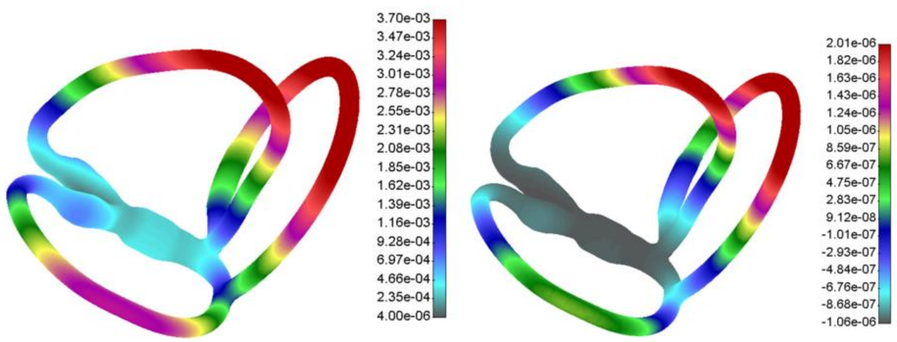

a) b)

Figure 5 The numerical result the velocity (a) and pressure (b) distribution along *the human membranous labyrinth during 1.5 m/s2 acceleration*

From the Figure 5, it can be concluded that the maximum value of the velocity and pressure is always in the PC duct, while the slightly lower values were recorded again in the HC duct. The highest pressure values of the 2.01e-06 Pa and 1.96e-06 Pa were recorded in the posterior and horizontal duct, respectively. It can be concluded that the acceleration change to which the human body was exposed, greatly affects the endolymph flow and pressure in membranous labyrinth. All of this has impact on small calcium carbonate crystals placed inside the semicircular canals, who are responsible for maintaining balance.

3. CONCLUSIONS

This paper showed the specific effect of whole body vibrations, to which the driver is exposed in the vehicle, on the vestibular system. A full 3D mathematical model of the semicircular canals with a full fluid-solid interaction of endolymph fluid flow and cupula deformation is investigated. Laboratory testing on a hydraulic pulsator determined the acceleration of the head via the accelerator, and then these values represented the input for the numerical model of the semicircular canals. On the example of two input accelerations, of 1 m/s^2 and 1.5 m/s^2, it is shown how the increase of acceleration affects the endolymph flow in these canals. An increase in the endolymph flow in the three semicircular canals leads to an increase in pressure which leads to an imbalance. For the first case the highest pressure of 1.61e-06 Pa was observed in posterior duct, while for the second case maximum value of pressure was 2.01e-06 Pa. This type of simulation may help medical doctors for better diagnostic procedures and therapy of balance disorder disease when high accelerations violates human health.

ACKNOWLEDGMENT

This research supported by the Ministry of Education, Science and Technological Development of Republic of Serbia through Grant TR 35041.

REFERENCES

[1] Mansfield, N.J.: "Human response to vehicle vibration", In: Gkikas, N. (Ed.), Automotive Ergonomics: Driver-vehicle interaction, Florida: CRC Press, 2013. pp. 77-96.

[2] Mansfield, N.J.: "Human Response to Vibration", Boca Raton, FL: CRC Press, 2005.

[3] Morgan, L.J.: "The influence of whole- body vibration and axial rotation on musculoskeletal discomfort of the neck and trunk", PhD Thesis, UK, Loughborough University, 2011.

[4] Paddan, G.S., Griffin, M.J.: "The transmission of translational seat vibration to the head – I. Vertical seat vibration", Journal of Biomechanics, 1988, Vol. 21, No. 3, pp. 191-197, doi: 10.1016/0021-9290(88)90169-8.

[5] Paddan, G.S., Griffin, M.J.: "The transmission of translational seat vibration to the head – II. Horizontal seat vibration", Journal of Biomechanics, 1988, Vol. 21, No. 3, pp. 199-206, doi: 10.1016/0021-9290(88)90170-4.

[6] ISO 2631-1: "Mechanical vibration and shock - Evaluation of human exposure to whole-body vibration - Part 1: General requirements, 1997.

[7] ISO 2631-5: "Mechanical vibration and shock - Evaluation of human exposure to whole-body vibration - Part 5: Method for evaluation of vibration containing multiple shocks, 2004.

[8] ISO 2631-4: "Mechanical vibration and shock- Evaluation of human exposure to whole-body vibration - Part 4: Guidelines for the evaluation of the effects of vibration and rotational motion on passenger and crew comfort in fixed-guideway transport systems ", Texas Tech University, 2001.

[9] Cullen, K., Sadeghi, S.: "Vestibular System", Scholarpedia, 2008, Vol.3, No. 1, p. 3313, doi: 10.4249/scholarpedia.3013.

[10] Tascioglu, A.B: "Brief Review of Vestibular Anatomy and Its Higher Order Projections", Neuroanatomy, 2005, Vol. 4, pp 24–27.

[11] Kojic, M., Filipovic, N., Stojanovic, B., Kojic, N: "Computer Modeling in Bioengineering - Theoretical Background, Examples and Software", John Wiley and Sons, Chichester, England, 2008.

[12] Hain, T.C., Helminski, J.O.: "Anatomy and Physiology of the Normal Vestibular System", In: Herdman, S.J., (Ed), Vestibular Rehabilitation. Philadelphia, PA: F.A. Davis Company, 2007.

MOBILITY & VEHICLE MECHANICS

DOI:10.24874/mvm.2022.48.01.05
UDC:629.3.038;0004.89

A NEURAL NETWORK-BASED CONTROL ALGORITHM FOR A HYDRAULIC HYBRID POWERTRAIN SYSTEM

Marko Kitanović [1], Slobodan Popović [2], Nenad Miljić [3], Predrag Mrđa[4]*

Received in September 2020 *Accepted in May 2022*
RESEARCH ARTICLE

ABSTRACT: Significant research efforts are invested in the quest for solutions that will increase the fuel economy and reduce the environmental impacts of ICE-powered vehicles. The main objective of the study presented in this paper has been to analyze and assess the performance of a control methodology for a parallel hydraulic hybrid powertrain system of a transit bus. A simulation model of the vehicle has been calibrated by analyzing data obtained during an experiment conducted in real-world traffic conditions aboard a Belgrade transit bus. A Dynamic Programming optimization procedure has been applied on the calibrated powertrain model and an optimal configuration that minimizes the fuel consumption has been selected. A Neural Network-based, implementable control algorithm has then been formed through a machine learning process involving data from the optimal, non-implementable Dynamic Programming-based control. Several Neural Network configurations have been tested to obtain the best fuel economy for the range of conditions encountered during normal transit bus operation. It has been shown that a considerable fuel consumption reduction on the order of 30% could be achieved by implementing such a system and calibration method.

KEY WORDS: *hydraulic hybrid, internal combustion engines, machine learning, dynamic programming, transit bus*

[1]*Marko Kitanović, PhD., Assist. prof., University of Belgrade, Faculty of Mechanical Engineering, Internal Combustion Engines Department, Kraljice Marije 16, 11120 Belgrade 35, Serbia, mkitanovic@mas.bg.ac.rs, https://orcid.org/0000-0002-3931-802X (*Corresponding author)*
[2]*Slobodan J. Popović, PhD, Assoc. prof., University of Belgrade, Faculty of Mechanical Engineering, Internal Combustion Engines Department, Kraljice Marije 16, 11120 Belgrade 35, Serbia, spopovic@mas.bg.ac.rs*
[3]*Nenad L. Miljić, PhD, Assoc. prof., University of Belgrade, Faculty of Mechanical Engineering, Internal Combustion Engines Department, Kraljice Marije 16, 11120 Belgrade 35, Serbia, nmiljic@mas.bg.ac.rs, https://orcid.org/0000-0003-3564-0203*
[4]*Predrag D. Mrđa, PhD, Assist. prof., University of Belgrade, Faculty of Mechanical Engineering, Internal Combustion Engines Department, Kraljice Marije 16, 11120 Belgrade 35, Serbia, pmrdja@mas.bg.ac.rs https://orcid.org/0000-0001-5534-6322*

UPRAVLJAČKI ALGORITAM ZA HIDRAULIČNI HIBRIDNI POGONSKI SISTEM ZASNOVAN NA NEURONSKOJ MREŽI

REZIME: Značajni istraživački napori ulažu se u potragu za rešenjima koja će povećati ekonomičnost goriva i smanjiti uticaj vozila na ICE pogon na životnu sredinu. Glavni cilj studije predstavljene u ovom radu je analiza i procena performansi metodologije upravljanja za paralelni hidraulični hibridni pogonski sistem tranzitnog autobusa. Simulacioni model vozila je kalibrisan analizom podataka dobijenih tokom eksperimenta sprovedenog u realnim saobraćajnim uslovima u beogradskom tranzitnom autobusu. Procedura optimizacije dinamičkog programiranja je primenjena na kalibrisani model pogonskog sklopa i izabrana je optimalna konfiguracija koja minimizira potrošnju goriva. Algoritam upravljanja koji se može primeniti, zasnovan na neuronskoj mreži, je zatim formiran kroz proces mašinskog učenja koji uključuje podatke iz optimalne, nesprovodljive kontrole zasnovane na dinamičkom programiranju. Nekoliko konfiguracija neuronske mreže je testirano da bi se postigla najbolja ekonomičnost goriva za niz uslova koji se javljaju tokom normalnog tranzitnog rada. Pokazalo se da se primenom ovakvog sistema i metode kalibracije može postići značajno smanjenje potrošnje goriva od oko 30%.

KLJUČNE REČI: *hidraulični hibrid, motori sa unutrašnjim sagorevanjem, mašinsko učenje, dinamičko programiranje, tranzitni autobus*

A NEURAL NETWORK-BASED CONTROL ALGORITHM FOR A HYDRAULIC HYBRID POWERTRAIN SYSTEM

Marko Kitanović, Slobodan Popović, Nenad Miljić, Predrag Mrđa

INTRODUCTION

Rising fuel prices and increasing awareness of environmental issues place greater emphasis on the quest for solutions that improve vehicle fuel economy and reduce harmful emissions. One of the many possible directions in that regard, and perhaps the most promising, is powertrain hybridization. Achieving improved fuel economy, lower emissions and a relatively low price without incurring penalties in performance, safety, reliability, and other vehicle-related aspects represents a great challenge for the automotive industry. For accommodating the hybrid powertrain demands of heavy vehicles, particularly those undergoing frequent deceleration and acceleration phases, the best solutions are those that can sustain very high power levels, such as the hydraulic hybrid or the ultracapacitors-based hybrid electric systems.

The main objective of the study presented in this paper is to analyze and assess the performance of a control methodology for a parallel hydraulic hybrid powertrain system. An experiment has been conducted on a transit bus circulating in real traffic and occupancy conditions in Belgrade, Serbia to assess the circumstances encountered in this particular type of transportation and in order to obtain the real driving cycle and the vehicle powertrain parameters necessary for conducting virtual analyses involving hybrid solutions. Data acquired during this experiment has been of crucial importance; effectively allowing us to conduct identification procedures on a set of powertrain parameters in order to calibrate the vehicle model used in the simulation. By successfully transferring the real-world physical conditions into computer code, a practically infinite number of numerical study possibilities has been opened. In the following section of this paper, methods applied during this research are presented, including an overview of the calibrated hybrid powertrain system simulation model used in this study. The methodology section also includes an overview of the Dynamic Programming method used to derive the optimal control law and to assess the ultimate fuel economy improvement potential of the hybrid powertrain system. Next, the details on the Artificial Neural Network (ANN) configurations used in this study to derive an implementable control algorithm are laid out.

The results and concluding remarks are presented in their respective sections, following the methodology section.

1. METHODOLOGY

The methods applied in this study are presented in the following subsections.

1.1 Hybrid Powertrain System Model

In order to calibrate the hybrid powertrain system model used in the study, an experiment was conducted on an Ikarbus IK206 transit bus circulating in real occupancy and traffic conditions. It was equipped with a MAN D2066 LUH 11 engine (10.5 dm^3, 6-cylinder, turbocharged diesel engine) and a Voith 864.5 automatic transmission. An autonomous data acquisition system based on National Instrument’s CompactRIO hardware platform and LabVIEW software has been designed for this purpose. The powertrain parameters were acquired by accessing the vehicle's J1939 CAN bus by means of a high-speed NI 9853 CAN module. The raw network stream has been logged and afterwards processed according to the SAE J1939 standard [1]. In order to obtain the GPS coordinates of the driving cycle, which are needed for determining the road slope, a Garmin GPS 18x 5 Hz receiver streaming NMEA messages was used. Suspension system pressure sensors have also been installed in order to log the vehicle mass during the experiment.

This experiment has been conducted for the duration of several weeks, during which a vast amount of highly valuable data has been collected. It has allowed the calibration of a MATLAB model of a conventional transit bus powertrain that has served afterwards as an input for Dynamic Programming (DP) optimization runs involving various hydraulic hybrid configurations. Rolling friction coefficients, aerodynamic friction coefficients, brake torque limits maps (Figure 1) and the engine BSFC (Figure 2), along with data concerning the gearbox, hydrodynamic torque converter and various drivetrain components among others, have been implemented into the base model. Detailed procedures and values can be found in [2, 3, 4].

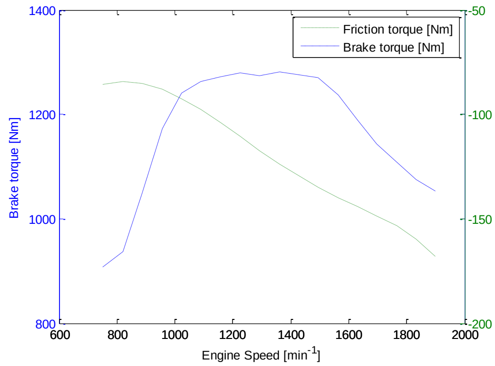

Figure 1 Max. engine brake torque and friction torque

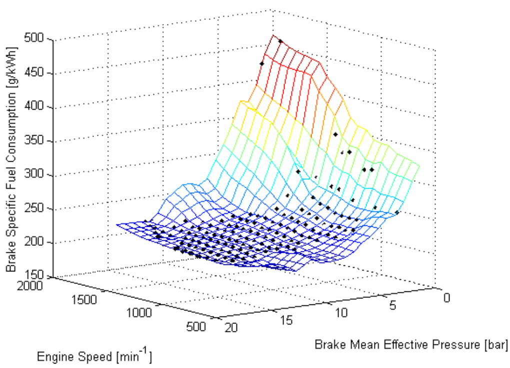

Figure 2 Brake Specific Fuel Consumption (BSFC) map

A model of a 250 cm^3, variable displacement swashplate axial piston pump (Rexroth A4VSO) has been used as the main hydraulic unit for recuperating the regenerative braking energy and subsequently providing traction to the vehicle during acceleration phases. A fixed ratio (1.2) gearbox is positioned between the pump and the vehicle drivetrain in order to match the operational range of the hydraulic unit with the engine speed range.

Compared to electrical batteries, hydro-pneumatic accumulators are characterized by a higher specific power and a lower specific energy. Its high specific power renders it suitable for heavy vehicles with frequent acceleration/deceleration phases. On the other hand, the low specific energy represents a disadvantage due to the limited braking recuperation potential and is a challenge that must be overcome in order to maximize the fuel economy benefits of the hydraulic hybrid system.

In this study, a two state simulation model of a hydro-pneumatic accumulator has been used. The first state variable - gas temperature *T* is derived from the gas energy equation [5]:

$$\left(\tau + \frac{m_f c_f}{h A_w}\right)\frac{dT}{dt} + T = T_w - \frac{T\tau}{c_v}\left(\frac{\partial p_g}{\partial T}\right)_v \frac{dv}{dt} \tag{1}$$

where

$$\tau = \frac{m_g c_v}{h A_w} \tag{2}$$

is the thermal time constant. Due to high pressures encountered in the accumulator, the ideal gas law cannot be used with sufficient accuracy. Instead, a Benedict-Webb-Rubin equation of state has been used for modelling the state of the nitrogen gas:

$$p_g = \frac{RT}{v} + \frac{1}{v^2}\left(B_0 RT - A_0 - \frac{C_0}{T^2}\right) + \frac{bRT - a}{v^3} + \frac{a\alpha}{v^6} + \frac{c}{v^3 T^2}\left(1 + \frac{\gamma}{v^2}\right)\exp^{-\gamma / v^2} \tag{3}$$

where the corresponding coefficients for nitrogen are taken from [6].

The second state variable, specific volume *v*, is derived from the continuity equation

$$\frac{dv}{dt} = \frac{Q_a}{m_g} \tag{4}$$

where Q_a is the pump/motor actual flow rate and m_g is the accumulator gas mass.

1.2 Dynamic Programming

Dynamic programming is a technique for solving optimal control problems. It has been used in this study to derive the optimal load distribution between the hydraulic pump/motor and the internal combustion engine, subject to various constraints and conditions, in order to minimize the fuel consumption.

Dynamic programming relies on the principle of optimality, which states that [7] "An optimal policy has the property that whatever the initial state and initial decision are, the remaining decisions must constitute an optimal policy with regard to the state resulting from the first decision."

By decomposing a control problem into segments or sub-problems, an optimal decision can be discovered at each stage, starting from the end and moving toward the initial instant. By defining the allowable final system state constraints, a DP algorithm starts with evaluating the optimal decision at the stage preceding the final stage that will result in the system reaching this final state at minimal cost. This is done by discretizing the state space, which results in a time-state space grid with nodes at which the cost is evaluated by sweeping the admissible control values, subject to state constraints. By proceeding backwards, an optimal control decision can be stated for each stage-state combination that will bring the system from the current stage-state point to the desired final state at minimal cost. By ultimately reaching the initial time stage, the cost-to-go and optimal control matrices are obtained, representing respectively the cost and optimal control decisions for each admissible stage-state combination. Mathematically, this can be stated through a recurrence relation [8]:

$$J^{*}_{N-K,N}\left(\vec{x}(N-K)\right)=\min_{u(N-K)}\begin{Bmatrix} g_D\left(\vec{x}(N-K),\vec{u}(N-K)\right)+ \\ +J^{*}_{N-(K-1),N}\left(\vec{a}_D\left(\vec{x}(N-K),\vec{u}(N-K)\right)\right)\end{Bmatrix} \tag{5}$$

By knowing $J^{*}_{N-(K-1),N}$, the optimal cost at the K-1 stage, the optimal cost for the stage K, $J^{*}_{N-K,N}$ can be determined, along with its corresponding control. Only one DP control variable has been used in this study: the load distribution *u*. In control phases, this control variable represents the engine to hydraulic motor torque ratio. During deceleration phases, it is defined as the ratio of hydraulic pump to friction brakes torque ratio. A generic MATLAB implementation of the DP algorithm has been used in this study [9].

1.3 Machine Learning

The DP-derived optimal control law is not implementable due to its dependency on future system states and conditions. This is why a machine learning algorithm based on ANN has been considered with the goal of trying to derive an implementable control algorithm that will yield near-optimal performance in a multitude of conditions observed in transit bus operation. An ANN was to be configured and trained using the optimal hybrid powertrain system load distribution obtained during the DP optimization runs for different representative driving cycles.

A NARX network (Figure 3) has been used in this research.

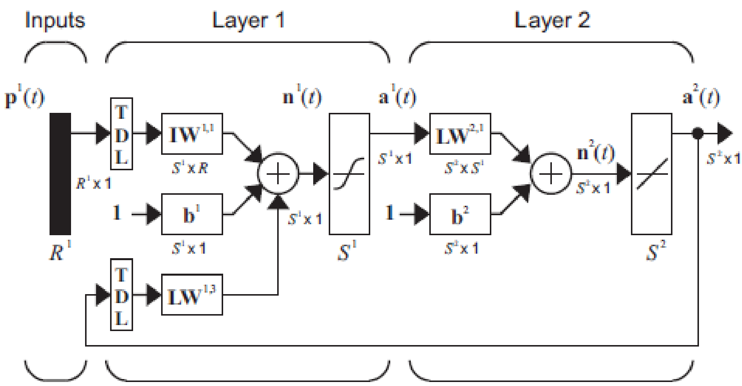

Figure 3 Nonlinear Autoregressive Network with eXogenous inputs (NARX) [10]

For exogenous inputs, a vector of 4 variables in total have been used – the instantaneous vehicle speed, the driveshaft torque as a representative of the actual powertrain load, the hydraulic machine normalized load and the hydro-pneumatic accumulator gas pressure. The motivation behind this choice lies in the necessity to give the ANN a sufficient amount of information regarding the state of the hybrid powertrain system with the intention to allow for the training process to be successfully accomplished, while providing parameters that would be relatively easy to acquire in a real-world scenario.

Optimal control data from the DP optimization routines that had been obtained for driving cycles in different traffic and vehicle occupancy conditions have been relied upon for the ANN training process. The characteristics of the driving cycles are presented in Tables 1 and 2. This set of data has then further been divided into the training dataset (comprising 70% of the set), the validation and test datasets (each containing 15% of the original data). The training set is used for weights and biases adjustment, while the validation set serves the purpose of stopping the training procedure before overfitting occurs. Specifically, the training process is set to be interrupted when no improvement in the validation MSE occurs for 6 consecutive iterations.

The Levenberg-Marquardt backpropagation technique has been employed for the training process, while the weights and biases of the network have been initialized using the Nguyen-Widrow initialization method.

Table 1 *Characteristics of driving cycles in direction 1 that have been selected for the ANN training process*

	Mean negative accel.	Mean positive accel.	Cycle durati-on	Mean vehi-cle mass	Total fuel mass consu-med	Vehicle stationa-ry periods fraction	Total stationary vehicle duration	Mean moving veloci-ty
cycle name	aneg	apos	Δt	mveh	mf	xtstat	Δtstat	vpos
[-]	[m/s^2]	[m/s^2]	[s]	[t]	[kg]	[%]	[s]	[m/s]
330001_05_1	-0.518	0.453	2769	18.85	6.54	33.2	919	6.748
370001_01_1	-0.407	0.414	3271	17.97	6.21	35.5	1160	5.924
290001_07_1	-0.521	0.488	3446	18.73	7.93	38.5	1327	5.902

Table 2 *Characteristics of driving cycles in direction 2 that have been selected for the ANN training process*

	Mean negative accel.	Mean positive accel.	Cycle duration	Mean vehicle mass	Total fuel mass consumed	Vehicle stationary periods fraction	Total stationary vehicle duration	Mean moving velocity
cycle name	aneg	apos	Δt	mveh	mf	xtstat	Δtstat	vpos
[-]	[m/s2]	[m/s2]	[s]	[t]	[kg]	[%]	[s]	[m/s]
330001_06_2	-0.487	0.457	2882	18.14	5.63	30.7	885	6.400
270001_11_2	-0.472	0.433	3377	19.40	5.60	38.4	1297	6.079
360001_09_2	-0.487	0.435	3755	17.64	6.41	40.7	1530	5.759

Different configurations of the network have been tested in order to find the one that will yield the closest performance to the reference control law obtained using the Dynamic Programming method.

2. RESULTS

The results of the research are presented in the following subsections. First, an analysis of the trained networks performance is provided, after which the selected ANN is applied on a set of driving cycles not used during the training process in order to analyze its fuel economy improvement results compared to the optimal solution calculated using DP.

2.1 ANN Training Performance

A total of 4 artificial neural network configurations using the NARX architecture have been considered in this investigation. The values for the input and feedback delays have been varied from 10 to 20 and 30 to 60, respectively, while 2 different layer size values of 4 and 8 neurons have been applied. For each set of applied configuration parameters, 10 training sessions have been attempted for the purpose of minimizing the influence of the random weights and biases initialization on the ANN performance. The actual number of valid NNs per configuration depends on the number of early training stop occurrences caused when breaching the upper limit on the *mu* parameter (regulating the training gain). The results shown in Figures 4 to 7 are obtained for a section of the original driving cycles that belongs to the test set data, i.e. not having been used in the training procedure. The load distribution from three different sources is plotted against time: the optimal hybrid powertrain load distribution (obtained through the DP calculation) is shown, along with the output of the trained individual ANN with the lowest testing Mean Square Error (MSE) and the combined average response of all the valid ANNs obtained by repeating the training process.

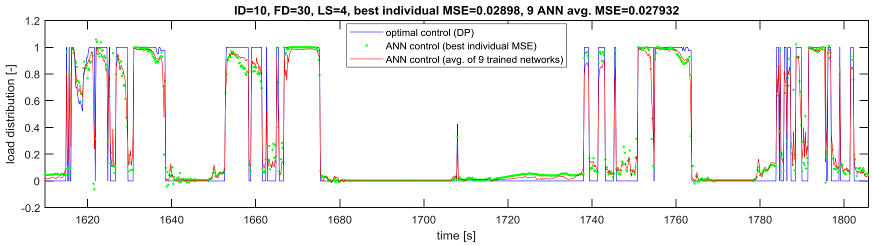

Figure 4 ANN control response for the best individual network, the average of the set of trained networks, compared to the optimal control (Input Delay of 10, Feedback Delay of 30, Layer Size of 4 neurons)

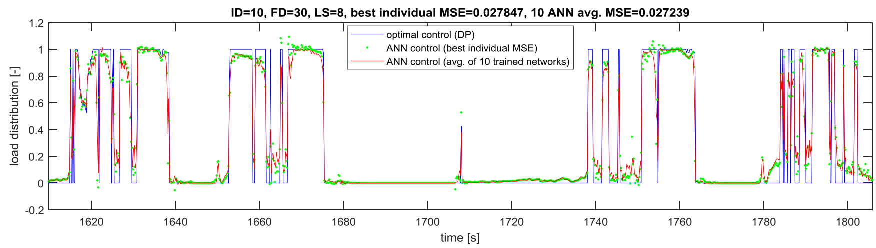

Figure 5 ANN control response for the best individual network, the average of the set of trained networks, compared to the optimal control (Input Delay of 10, Feedback Delay of 30, Layer Size of 8 neurons)

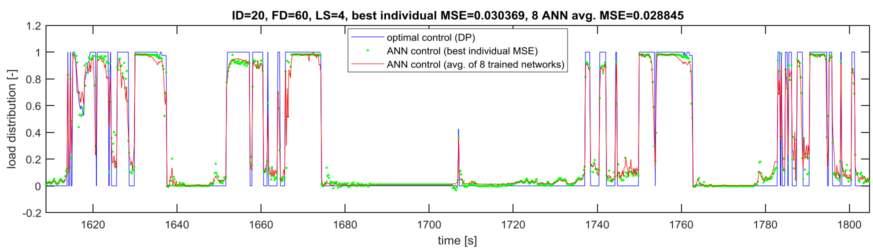

Figure 6 ANN control response for the best individual network, the average of the set of trained networks, compared to the optimal control (Input Delay of 20, Feedback Delay of 60, Layer Size of 4 neurons)

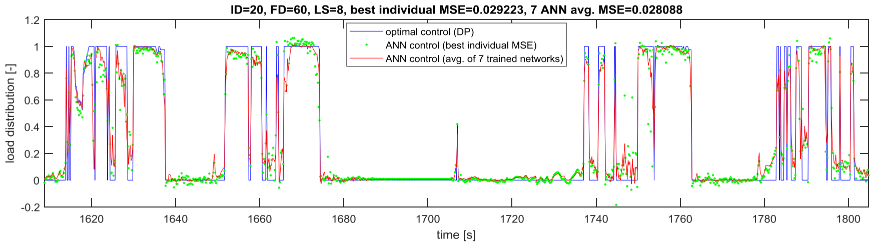

Figure 7 ANN control response for the best individual network, the average of the set of trained networks, compared to the optimal control (Input Delay of 20, Feedback Delay of 60, Layer Size of 8 neurons)

Figures 4 and 5 show data that has been obtained for the lower input and feedback delay sizes (10 and 30, respectively). It can be said that even for the simplest NARX configuration considered in this research, the ANN control yields acceptable results. The individual ANN (from this configuration variation batch) with the best achieved testing performance (i.e. the lowest MSE) tracks the optimal load distribution on the driving cycle section shown quite well, even though the control parameter overshoots the upper bound or does not quite reach the required optimal level repeatedly. The lowest individual MSE obtained by taking into account the testing set data (representing 15% of the whole dataset) is on the order of 0.029. By combining the outputs of 9 trained ANN with the simplest configuration, the resulting MSE drops by approximately 3.6%, with visibly better tracking of the optimal load distribution on the test data section shown in Figure 4. Overshoots are dampened and the oscillations where the optimal control value is constant are moderated.

By increasing the number of neurons in the hidden layer of the NARX from 4 to 8, the individual ANN with the best performance gets its MSE lowered by 3.9%. In this case, overshoots occur at different instants of time but the ANN control yields better tracking at extreme reference values. By combining the outputs of 10 trained networks and calculating the average, the MSE is reduced by only 2.2% compared to the best individual ANN MSE and by 2.5% compared to the corresponding MSE of the NARX with 4 neurons.

By increasing the input and feedback delay sizes by a factor of 2, it can be seen that the best individual and combined ANN performance drops compared to the NARX with input/feedback delays of 10/30 and the layer size of 8 neurons. Specifically, the best individual ANN yields an MSE that is 9% higher than the corresponding MSE of the NARX with the best configuration. The effect of the increase in delay sizes is an increase in best individual ANN MSE of 4.8% for the NARX with 4 neurons. By combining the outputs of the 8 valid ANN of this case and calculating the average control value, a reduction in the MSE of 5% is achieved. By increasing the number of neurons from 4 to 8, a marginal improvement of approximately 3.8% is achieved in best individual MSE and an improvement of 2.6% in combined ANN MSE.

2.2 ANN Control Performance

In this subsection of the article, the results of the application of the ANN control on a hydraulic hybrid transit bus powertrain system simulation are shown and compared against the optimal control results obtained using the dynamic programming algorithm. The individual ANN with the best control variable matching (Input/Feedback Delay of 10/30 and with layer size of 8) has been chosen to perform the analysis.

In total, 6 different driving cycles have been considered for evaluating the performance of the selected ANN control, three for each route direction. All six cycles have been obtained in real traffic and occupancy conditions. For each route direction, one cycle per congestion state has been chosen in order to analyze the impact of the ANN control on the fuel consumption improvement potential for different driving conditions. Indeed, all driving cycles acquired during the experiment have been divided into three categories based on the total duration of the runs. These categories have been further divided into three subcategories according to the values of the mean vehicle positive velocity. For each total run duration category, one cycle with moderate positive vehicle speed value has been chosen. In the end, a cycle representative of low, moderate and high congestion states has been selected for both route directions. It should be noted that the cycles used for the validation of the control methodology have not been part of the ANN training selection.

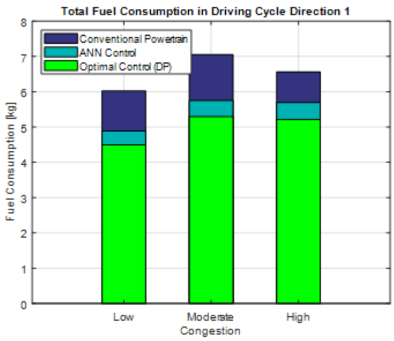

Figure 8 Absolute fuel consumption comparison for the driving cycles in direction 1

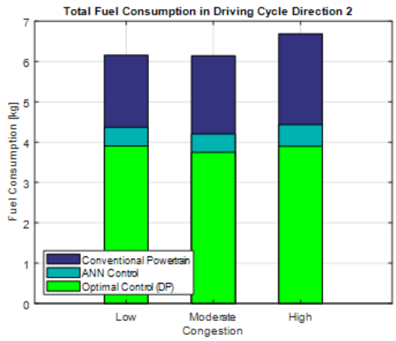

Figure 9 Absolute fuel consumption comparison for the driving cycles in direction 2

Figures 8 and 9 show the absolute fuel consumption for the conventional powertrain, along two other values obtained by simulating the hybrid system solution – one using the optimal control derived by the dynamic programming algorithm and the other realized using the selected ANN control. Calculations have been carried out for the three traffic conditions mentioned earlier and for both driving cycle directions. Maximum absolute fuel consumption savings occur in the route direction 2, primarily due to the difference in the terrain elevations of the bus terminal stations. Indeed, the starting "Crveni Krst" terminal station is located approximately 60 m above the destination of the driving cycle direction 2 – the "Zemun Bačka" terminal station, allowing greater potential energy of the vehicle to be harnessed by the use of the hybrid powertrain system. Maximum achievable fuel consumption reductions range from 1.3 to 1.7 kg in the route direction 1, while savings on the order of 2.2 to 2.8 kg can be achieved in the direction 2 in the optimal case. The savings achieved by using an implementable control algorithm range from 0.86 to 1.3 kg in direction 1, and 1.8 to 2.2 kg in route direction 2. The fuel consumption improvement relative to the conventional powertrain system is shown in Figures 10 and 11 for all six driving cycles considered in this ANN control validation investigation. The least relative amount of fuel saved is achieved for the most congested cycle in direction 1, where only 20.5% can be optimally achieved. Using the implementable ANN control algorithm, 13.2% of fuel can be saved. Ideally, approximately 25% of the fuel used for powering the conventional powertrain system may be saved in low and moderate congestion states in direction 1. The ANN control can cut back approximately 18.5% of the fuel consumed in a non-hybrid transit bus. The values achieved in direction 2 show a different trend. Namely, potential fuel savings rise with increasingly congested traffic conditions, with over 40% of fuel savings ideally achieved for the most congested driving cycle. The least amount of fuel consumption improvement in driving cycle direction 2 reaches a figure of over 36%, which is significantly higher than the most favorable case in direction 1. The range of values representing fuel savings achievable using the selected ANN control is from 29.1% for the least, to 33.7% for the most congested state.

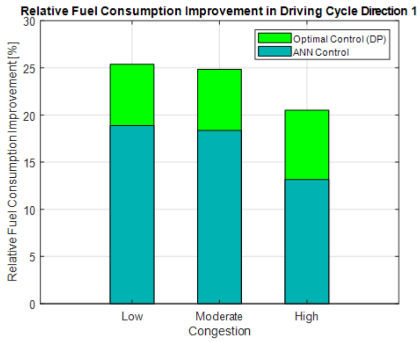

Figure 10 Relative fuel consumption improvement compared to the conventional powertrain system for the driving cycles in direction 1

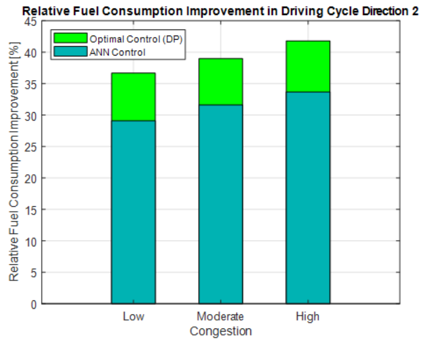

Figure 11 Relative fuel consumption improvement compared to the conventional powertrain system for the driving cycles in direction 2

By analyzing the optimal fuel consumption savings that could ideally be achieved and the values obtained using the ANN control, it can be concluded that the proposed implementable control algorithm yields a good performance. Over 64% of the potential fuel savings can be achieved by using the ANN control in the most congested driving conditions in direction 1. In the most favorable case (in the most congested conditions in direction 2), over 80% of the maximally achievable fuel consumption reduction can be accomplished by using the suboptimal, implementable control algorithm.

3. CONCLUSIONS

An implementable, artificial neural network based control algorithm has been devised to control the load distribution in a parallel, hydraulic hybrid powertrain system for a transit bus. A physical experiment involving the use of a transit bus circulating in real traffic and occupancy conditions as part of the Belgrade's public transportation service has been conducted in order to acquire the data needed to calibrate a simulation model of the powertrain system. This endeavor has also allowed to acquire the driving cycles in differing traffic congestion states, a prerequisite for training and validating the proposed ANN control.

By using a NARX ANN, up to 80% of the ultimate fuel consumption improvement potential obtained using a non-implementable optimization algorithm can be achieved. Further research efforts shall be invested in order to analyze the conditions required for closing the gap to the optimal solution.

ACKNOWLEDGMENT

The research presented in this paper is conducted in the framework of the research project TR35042, titled Research and Development of Alternative Fuel and Drive Systems for Urban Buses and Refuse Vehicles with Regard to the Improvements of Energy Efficiency and Environmental Characteristics, which is funded by the Ministry of Education, Science and Technological Development.

REFERENCES

[1] "Vehicle Application Layer, SAE J1939/71_200412", Truck Bus Control and Communications Network Committee, Society of Automotive Engineers, 2004.

[2] Kitanović, M.N., Mrđa, P., Popović, S., Miljić, N.: "Fuel economy comparative analysis of conventional and ultracapacitors-based, parallel hybrid electric powertrains for a transit bus", Proceedings, 5th International Congress Motor Vehicles & Motors, Kragujevac, Serbia, 2014, pp. 258-267.

[3] Kitanović, M.N., et al.: "Dynamic programming study of a hybrid electric powertrain system for a transit bus", Proceedings, 18th Symposium on Thermal Science and Engineering of Serbia, Sokobanja, 2017, pp. 988-997.

[4] Kitanović, M., Mrđa, P., Petrović, V., Miljić, N., Popović, S., Tomić, M.: "A simulation study of fuel economy improvement potentials of a transit bus", Proceedings, 24th International Automotive Conference Science and Motor Vehicles, Belgrade, Serbia, 2013, pp. 56-67.

[5] Pourmovahed, A., et al.: "Modeling of a hydraulic energy regeneration system-part i: analytical treatment", Journal of Dynamic Systems, Measurement, and Control, 1992, Vol. 114, No. 1, pp. 155-159, doi: 10.1115/1.2896497.

[6] Pourmovahed, A.: "Energy storage capacity of gas-charged hydraulic accumulators", Proceedings, 23rd Thermophysics, Plasmadynamics and Lasers Conference, San Antonio, Texas, USA, 1988, pp. 1-11.

[7] Bellman, R.E., Dreyfus, S.E.: "Applied Dynamic Programming", Princeton University Press, Princeton, N.J. USA, 1962.

[8] Kirk, D.E.: "Optimal Control Theory: An Introduction", Dover Publications, Mineola, N.Y., USA, 2004.

[9] Sundstrom, O., Guzzella, L.: "A Generic Dynamic Programming Matlab Function", Proceedings (2009 IEEE control applications (CCA) & intelligent control (ISIC)), 3rd IEEE Multi-Conference on Systems and Control, St. Petersburg, Russia, 2009, pp. 1625-1630.

[10] Beale, M.H., Hagan, M.T. Demuth, H.B.: "Deep Learning Toolbox. User's Guide", MathWorks, 2019.

NOTIFICATION TO AUTHORS

The Journal MVM publishes original papers which have not been previously published in other journals. This is responsibility of the author. The authors agree that the copyright for their article is transferred to the publisher when the article is accepted for publication.

The language of the Journal is English.

Journal ***Mobility & Vehicles Mechanics*** is at the SSCI list.

All submitted manuscripts will be reviewed. Entire correspondence will be performed with the first-named author.

Authors will be notified of acceptance of their manuscripts, if their manuscripts are adopted.

INSTRUCTIONS TO AUTHORS AS REGARDS THE TECHNICAL ARRANGEMENTS OF MANUSCRIPTS:

Abstract is a separate Word document, "*First author family name_ABSTRACT.doc*". Native authors should write the abstract in both languages (Serbian and English). The abstracts of foreign authors will be translated in Serbian.

This document should include the following: 1) author's name, affiliation and title, the first named author's address and e-mail – for correspondence, 2) working title of the paper, 3) abstract containing no more then 100 words, 4) abstract containing no more than 5 key words.

The manuscript is the separate file, „*First author family name_Paper.doc*" which includes appendices and figures involved within the text. At the end of the paper, a reference list and eventual acknowledgements should be given. References to published literature should be quoted in the text brackets and grouped together at the end of the paper in numerical order.

Paper size: Max 16 pages of B5 format, excluding abstract
Text processor: Microsoft Word
Margins: left/right: mirror margin, inside: 2.5 cm, outside: 2 cm, top: 2.5 cm, bottom: 2 cm
Font: Times New Roman, 10 pt
Paper title: Uppercase, bold, 11 pt
Chapter title: Uppercase, bold, 10 pt
Subchapter title: Lowercase, bold, 10 pt
Table and chart width: max 125 mm
Figure and table title: Figure _ (Table _): Times New Roman, italic 10 pt

Manuscript submission: application should be sent to the following e-mail:

mvm@kg.ac.rs ; lukicj@kg.ac.rs
or posted to address of the Journal:
University of Kragujevac – Faculty of Engineering
International Journal M V M
Sestre Janjić 6, 34000 Kragujevac, Serbia

The Journal editorial board will send to the first-named author a copy of the Journal offprint.

OBAVEŠTENJE AUTORIMA

Časopis MVM objavljuje orginalne radove koji nisu prethodno objavljivani u drugim časopisima, što je odgovornost autora. Za rad koji je prihvaćen za štampu, prava umnožavanja pripadaju izdavaču.

Časopis se izdaje na engleskom jeziku.

Časopis ***Mobility & Vehicles Mechanics*** se nalazi na SSCI listi.

Svi prispeli radovi se recenziraju. Sva komunikacija se obavlja sa prvim autorom.

UPUTSTVO AUTORIMA ZA TEHNIČKU PRIPREMU RADOVA

Rezime je poseban Word dokument, "*First author family name_ABSTRACT.doc*". Za domaće autore je dvojezičan (srpski i engleski). Inostranim autorima rezime se prevodi na srpski jezik. Ovaj dokument treba da sadrži: 1) ime autora, zanimanje i zvanje, adresu prvog autora preko koje se obavlja sva potrebna korespondencija; 2) naslov rada; 3) kratak sažetak, do 100 reči, 4) do 5 ključnih reči.

Rad je poseban fajl, „*First author family name_Paper.doc*" koji sadrži priloge i slike uključene u tekst. Na kraju rada nalazi se spisak literature i eventualno zahvalnost. Numeraciju korišćenih referenci treba navesti u srednjim zagradama i grupisati ih na kraju rada po rastućem redosledu.

Dužina rada: Najviše 16 stranica B5 formata, ne uključujući rezime
Tekst procesor: Microsoft Word
Margine: levo/desno: mirror margine; unurašnja: 2.5 cm; spoljna: 2 cm, gore: 2.5 cm, dole: 2 cm
Font: Times New Roman, 10 pt
Naslov rada: Velika slova, bold, 11 pt
Naslov poglavlja: Velika slova, bold, 10 pt
Naslov potpoglavlja: Mala slova, bold, 10 pt
Širina tabela,dijagrama: max 125 mm
Nazivi slika, tabela: Figure __ (Table _): Times New Roman, italic 10 pt

Dostavljanje rada elektronski na E-mail: **mvm@kg.ac.rs ; lukicj@kg.ac.rs**

ili poštom na adresu Časopisa
Redakcija časopisa M V M
Fakultet inženjerskih nauka
Sestre Janjić 6, 34000 Kragujevac, Srbija

Po objavljivanju rada, Redakcija časopisa šalje prvom autoru jedan primerak časopisa.

MVM *Editorial Board*
University of Kragujevac
Faculty of Engineering
Sestre Janjić 6, 34000 Kragujevac, Serbia
Tel.: +381/34/335990; Fax: + 381/34/333192
www.mvm.fink.rs